applied sciences

MDPI

Article

Analysis of the Influence of Antenna Arrangement Parameters on the Aerodynamic Performance of Telecommunication Towers

Yaya Jia [1,2,3,*], Jiachen Huang [1], Qingkuan Liu [1,2,3], Zonghan Zhao [1] and Menghui Dong [1]

[1] School of Civil Engineering, Shijiazhuang Tiedao University, Shijiazhuang 050043, China; 1202101022@student.stdu.edu.cn (J.H.); qk@stdu.edu.cn (Q.L.); zzh546429965@163.com (Z.Z.); dddmh12138@163.com (M.D.)
[2] State Key Laboratory of Mechanical Behavior and System Safety of Traffic Engineering Structures, Shijiazhuang 050043, China
[3] Innovation Center for Wind Engineering and Wind Energy Technology of Hebei Province, Shijiazhuang 050043, China
* Correspondence: jiayaya@stdu.edu.cn; Tel.: +86-187-1295-7255

Abstract: With the widespread adoption of 5G telecommunication networks, to reduce construction costs, it has become necessary to add new equipment or antennas to existing 4G and 3G telecommunication towers. This significantly changes the original aerodynamic shape of the towers, leading to a substantial increase in the wind load, which may exceed the original structure's bearing capacity and pose a threat to the structure's safety. This study employed three-dimensional numerical simulation methods to systematically investigate the impact of various antenna arrangement parameters, such as the arrangement number, arrangement form, and arrangement layers, on the wind load characteristics of telecommunication towers. The findings revealed that the antenna arrangement form significantly affects the sensitivity of the telecommunication tower's wind load to the wind direction, with more uniform antenna arrangements resulting in less sensitivity. Compared to the drag coefficient and the windward base overturning moment coefficient, the tower's lateral force coefficient and the crosswind base overturning moment coefficient are more sensitive to changes in the wind direction. The change patterns in the tower's overturning force coefficient and overturning moment coefficient with the antenna arrangement number are essentially the same. However, as the antenna arrangement number increases, the growth rate of the tower's overturning moment coefficient is about twice that of the overturning force coefficient. The tower's overturning force coefficient increases approximately linearly with the increase in antenna arrangement layers, while the tower's overturning moment coefficient exhibits a nonlinear increase with the increase in antenna arrangement layers. The rate of increase in the wind load with the antenna arrangement layers is significantly greater than that with the antenna arrangement number. Thus, to reduce wind load, it is advisable in practical engineering applications to increase the antenna arrangement number per layer, thereby reducing the antenna arrangement layers. The study also summarized a calculation method for the structural wind load of telecommunication towers, taking into account the influence of antenna arrangement parameters, providing a reliable basis for the structural design and safety assessment of telecommunication towers in practical engineering.

Keywords: telecommunication tower; antenna; arrangement parameter; numerical simulation; wind load

Citation: Jia, Y.; Huang, J.; Liu, Q.; Zhao, Z.; Dong, M. Analysis of the Influence of Antenna Arrangement Parameters on the Aerodynamic Performance of Telecommunication Towers. *Appl. Sci.* **2024**, *14*, 2538. https://doi.org/10.3390/app14062538

Academic Editor: Maciej Dutkiewicz

Received: 4 February 2024
Revised: 12 March 2024
Accepted: 12 March 2024
Published: 18 March 2024

1. Introduction

Slender tower structures are widely used, such as in street lights, telecommunication towers, masts, etc. These structures are characterized by small cross-sections, large aspect ratios, and high flexibility, making them wind-sensitive structures. Wind load is one of the primary controlling loads in the design of slender tower structures and has a critical impact on their safety.

Wind tunnel testing is a reliable method to obtain the aerodynamic characteristics of slender tower-like structures. Kim et al. [1], using wind tunnel tests, found that polygonal towers have better aerodynamic stability and vibrational response than traditional circular towers. Mannini et al. [2] focused their wind tunnel experimental studies on the aerodynamic loads during the pre-assembly stage of offshore wind turbine towers, discovering that the height of the tower significantly impacts aerodynamic loads. Azzi et al. [3] used aeroelastic models to assess the response of multi-span transmission line systems under various wind speeds and directions, indicating the differences in aerodynamic response between multi-span systems and individual lattice towers. Prud et al. [4] studied the aerodynamic coefficients of single cylindrical bodies and developed a local calculation method to compute the wind loads on lattice structures. Martín et al. [5] measured the drag coefficient and interference factors of square-section lattice towers with dish antennas through wind tunnel experiments, finding that interference factors depend on wind direction and the position of antennas on the tower section. Torrielli et al. [6] explored the uncertainty in the response of tower structures to storm oscillations, emphasizing the importance of the accurate estimation of wind speed extremes, structural damping, and aerodynamic coefficients in assessing tower responses. Xia et al. [7] conducted wind tunnel tests to measure the wind loads on a model of the Foshan TV tower, comparing the experimental results with those calculated using the complete quadratic combination method.

In recent years, many scholars both domestically and internationally have begun to research the wind resistance of slender tower structures using numerical simulation methods. Battista et al. [8] used a 3D computational model to assess the aerodynamic behavior and structural stability of the Brasília Telecommunications Tower, finding that antennas and brackets significantly affect aerodynamic forces and response amplitudes. Winterstein et al. [9] proposed a high-fidelity simulation method, which was validated against field measurement data, demonstrating its potential in assessing transient effects induced by wind on slender structures. Cheng et al. [10] introduced a new method for controlling the along-wind vibration of chimneys by adjusting the lining, which was proven to be more effective than traditional dampers through validation with beam models and finite element shell models. Poddaeva et al. [11] combined numerical simulation and wind tunnel testing to study the effects of wind on lattice structures, exploring the vortex resonance excitation mechanisms of these structures. Fu et al. [12] proposed a method for the wind-resistant dimensional optimization of lattice structures, emphasizing the importance of geometric nonlinear analysis and constraints of nonlinear critical load factors. Ribeiro et al. [13] analyzed wind-induced fatigue in guyed lattice steel towers, pointing out that the modular connection area is the most critical part for fatigue damage. Qin et al. [14] conducted studies on the aerodynamic performance of single-pole telecommunication towers using both wind tunnel tests and numerical simulations, demonstrating that numerical simulation techniques can serve as an effective alternative to wind tunnel tests for assessing the aerodynamic behavior of single-pole telecommunication towers. Kumar et al. [15] compared the aerodynamic characteristics of single-pole and self-supporting telecommunication towers at different heights, finding that self-supporting towers have smaller lateral displacements under the same loads.

Although the study of wind load characteristics on slender towers has always been a focal point of interest among scholars both domestically and internationally, existing research and industry standards mostly target individual tower structures [16–23]. With the acceleration of modernization, some slender tower structures need to have ancillary facilities installed around them to meet usage requirements. The arrangement of these ancillary facilities significantly impacts the wind load characteristics of slender towers. For instance, since 2019, with the widespread adoption of 5G networks, to reduce construction costs, most 5G telecommunication towers have been established by adding new equipment or antennas to existing 4G and 3G telecommunication towers [24–30]. Adding telecommunication antennas and other ancillary facilities to telecommunication towers significantly alters their original aerodynamic shape, leading to a substantial increase in wind loads, which

might exceed the original structural capacity and threaten the safety of the structure. In light of these considerations, existing research, while extensive, offers limited guidance on assessing the impact of ancillary facilities such as antennas on the wind loads experienced by slender towers. Therefore, this study employed three-dimensional numerical simulation methods to systematically analyze the impact of various antenna arrangement parameters, such as arrangement number, arrangement form, and arrangement layers, on the structural wind loads of telecommunication towers. It also summarized a calculation method for these wind loads considering the impact of antenna arrangement parameters, providing a reliable basis for the structural design and safety assessment of telecommunication towers in practical engineering applications.

2. Numerical Calculation Method for Telecommunication Towers

2.1. Numerical Calculation Model for Telecommunication Towers

The subject of the study was an actual single-pipe telecommunication tower, with a height of H = 35.0 m. The diameter of the circumscribed circle at the top is D_1 = 0.5 m, and at the bottom is D_2 = 1.0 m. Through surveying, it was found that the tower can accommodate up to three layers of telecommunication antennas, with each layer exhibiting the same antenna arrangement number and antenna arrangement form, up to a maximum of six per layer. Therefore, the total antenna arrangement number on the tower can range from 1 to 18. The top surface elevation of the first layer of antennas is at 1.0H, the second at 0.85H, and the third at 0.71H. Figure 1 shows the mesh of the telecommunication tower and the schematic of the wind loads when 18 antennas are arranged [31].

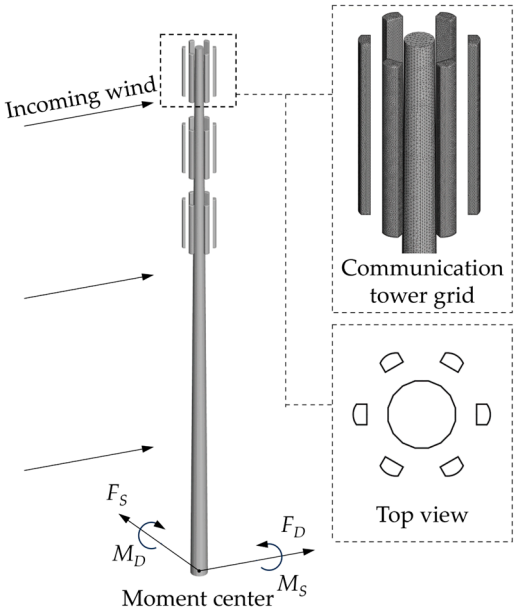

Figure 1. Schematic of the telecommunication tower mesh and wind loads [31].

Since the antennas were symmetrically arranged, the wind loads on the surface of the telecommunication tower structure were calculated for all wind directions from 0° to 180°. This primarily included the drag force F_D acting in the windward direction on the entire tower, the lateral force F_S in the crosswind direction, the windward base overturning moment M_D, and the crosswind base overturning moment M_S, with the moment center located at the center of the tower's base. By non-dimensionalizing, we obtained the drag coefficient C_D, the lateral force coefficient C_S, the windward base overturning moment coefficient C_{MD}, and the crosswind base overturning moment coefficient C_{MS}, as specifically shown in Equations (1)–(4):

Drag coefficient:

$$C_D = \frac{F_D}{0.5\rho {U_{10}}^2 A} \tag{1}$$

Lateral force coefficient:

$$C_S = \frac{F_S}{0.5\rho {U_{10}}^2 A} \tag{2}$$

Windward base overturning moment coefficient:

$$C_{MD} = \frac{M_D}{0.5\rho {U_{10}}^2 D H^2} \tag{3}$$

Crosswind base overturning moment coefficient:

$$C_{MS} = \frac{M_S}{0.5\rho {U_{10}}^2 D H^2} \tag{4}$$

where A represents the windward surface area of the telecommunication tower (m^2); ρ is the air density (kg/m^3); U_{10} is the reference wind speed at a height of 10.0 m (m/s); D is the average value of the diameters of the circumscribed circles of the top and bottom surfaces of the telecommunication tower (m); H is the height of the telecommunication tower (m).

By superimposing the drag coefficient and the lateral force coefficient, the overturning force coefficient C_F was obtained; by superimposing the windward base overturning moment coefficient and the crosswind base overturning moment coefficient, the overturning moment coefficient C_M was derived, as specifically shown in Equations (5) and (6):

Overturning force coefficient:

$$C_F = \sqrt{{C_D}^2 + {C_S}^2} \tag{5}$$

Overturning moment coefficient:

$$C_M = \sqrt{{C_{MD}}^2 + {C_{MS}}^2} \tag{6}$$

2.2. Computational Domain and Mesh Division Strategy

The accuracy of numerical simulation results is directly influenced by the selection of the computational domain. The scale independence of the domain was verified by choosing domains of different sizes. As shown in Figure 2, the computational domain's inlet is located $6H$ away from the telecommunication tower, the outlet of the flow domain is at $12H$, and the left and right boundaries are $3H$ from the tower, with the domain's height set to $6H$, where H represents the height of the telecommunication tower. The mesh division of the flow domain is shown in Figure 3. To enhance the accuracy of the numerical simulation, an unstructured mesh was used to refine the mesh around the tower cylinder and antennas. This involved the addition of an inflation layer near the walls of the tower cylinder and antennas to address areas of high-stress concentration. The mesh of the inflation layer, which was achieved by stretching along the boundary normals, improved the mesh accuracy and consisted of a combination of triangular and quadrilateral meshes. The distance of the first layer of mesh nodes to the wall surfaces satisfies $y^+ \leq 5$. The mesh around the telecommunication tower is shown in Figure 4.

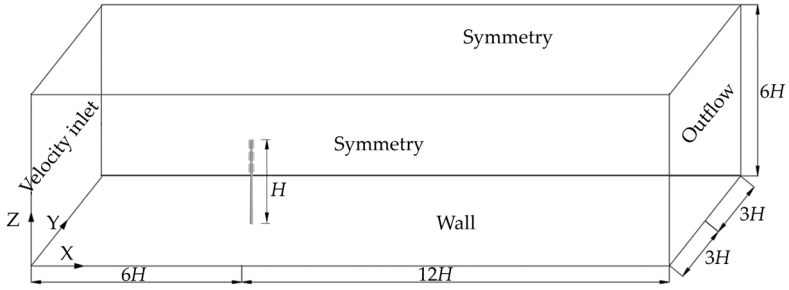

Figure 2. Diagram of the computational domain dimensions.

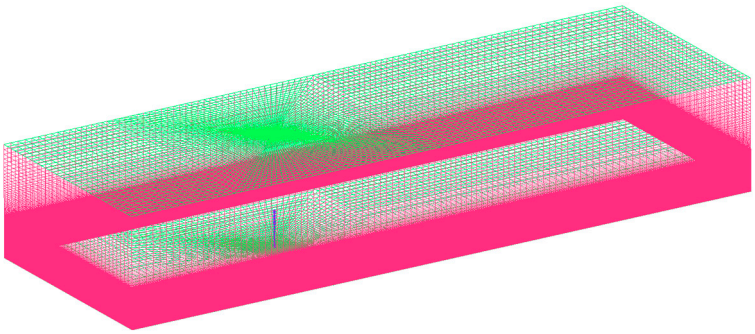

Figure 3. Mesh map of the flow domain.

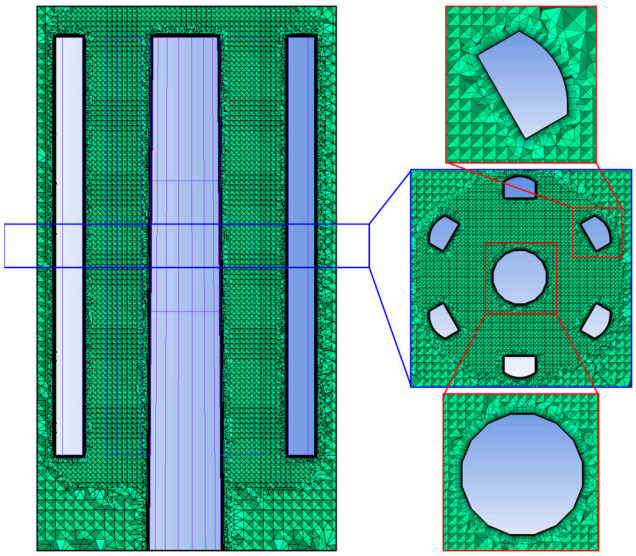

Figure 4. Mesh around the tower cylinder and antennas.

To ensure the simulation results were not affected by the quality of the mesh, while also considering computational costs, this paper conducted a grid independence verification. For both the bare tower condition without antennas and the condition with a single layer of six antennas arranged, three different mesh schemes of varying densities and numbers of elements were divided for each condition, as shown in Tables 1 and 2, which present the calculated average drag coefficient and lateral force coefficient for the telecommunication tower. With the increase in the number of elements, the average lateral force coefficient of the tower is very small, approximately zero; the drag coefficient gradually increases. In Tables 1 and 2, the relative errors for the drag coefficient between mesh scheme 1 and scheme 2 are 3.8% and 5.4%, respectively. Furthermore, the differences in the drag coefficient between scheme 2 and scheme 3 are even smaller, with relative errors of only

0.8% and 1.1%, respectively. Therefore, to obtain accurate simulation results within the constraints of limited computational resources and time, the second mesh scheme was chosen for calculations. The total number of elements used in this scheme ranges from 4.34 to 10.7 million.

Table 1. Mesh independence verification data table for the bare tower condition without antennas.

Mesh Scheme	Number of Elements (Million)	Lateral ForceCoefficient	Drag Coefficient	Change Rate of Drag Coefficient
1	3.34	2.8×10^{-2}	0.690	-
2	4.34	8.0×10^{-4}	0.716	3.8%
3	5.52	8.2×10^{-5}	0.722	0.8%

Table 2. Mesh independence verification data table for the condition with a single layer of 6 antennas arranged.

Mesh Scheme	Number of Elements (Million)	Lateral ForceCoefficient	Drag Coefficient	Change Rate of Drag Coefficient
1	4.87	1.14×10^{-2}	0.795	-
2	6.03	2.95×10^{-3}	0.838	5.4%
3	7.24	1.09×10^{-5}	0.847	1.1%

2.3. Numerical Calculation Method and Boundary Conditions

The coupling of pressure and velocity in the numerical simulation was addressed using the SIMPLE algorithm, and the control equations were solved using the segregated method. The SST k-ω turbulence model was selected for its wide applicability, high accuracy, and reliability among two-equation models. The convection terms of the control equations employed a second-order upwind scheme. The convergence criteria for the calculations were set with a residual value of 10^{-6}, while the overturning force, overturning moment, and the complex flow structures around the telecommunication tower were monitored in real time. These elements collectively served as the standards for determining the convergence of the computations.

In this study, these computations were used to solve the incompressible Reynolds-averaged Navier–Stokes equations and shear-stress transport (SST) k-ω turbulence model to obtain accurate results. The model has been proven to perform well in simulations of the attached flow to the structure [32]. In this study, the SST k-ω turbulence model was used in the wall boundary layer. The SST k-ω model was developed by Menter [33] to blend the robust and accurate formulations of the k-ω model in the near-wall region with the free-stream independence of the k-ε model in the far field. To avoid the free-stream sensitivity of the standard k-ω model, elements of the ω-equation and the ε-equation were combined.

For an unsteady state, in-viscous, incompressible three-dimensional turbulent flow, the equations of mass and momentum are written below [34].

Mass equation:

$$\frac{\partial \rho}{\partial t} + \nabla \cdot (\rho \vec{V}) = 0 \tag{7}$$

Momentum equation:

$$\frac{\partial (\rho \vec{V})}{\partial t} + \nabla \cdot (\rho \vec{V} \vec{V}) = -\nabla p + \nabla \cdot (\bar{\bar{\tau}}) \tag{8}$$

The transport equations for the SST k-ω model are given by

$$\frac{\partial(\rho k)}{\partial t} + \frac{\partial(\rho k v_i)}{\partial x_i} = \frac{\partial}{\partial x_j}\left(\Gamma_k \frac{\partial k}{\partial x_j}\right) + G_k - Y_k + S_k \tag{9}$$

$$\frac{\partial(\rho \omega)}{\partial t} + \frac{\partial(\rho \omega v_j)}{\partial x_j} = \frac{\partial}{\partial x_j}\left(\Gamma_\omega \frac{\partial \omega}{\partial x_j}\right) + G_\omega - Y_\omega + D_\omega + S_\omega \tag{10}$$

where k is the turbulent kinetic energy; ω is the specific dissipation rate; ρ is the fluid density; t is the time; V is the instantaneous velocity; p is the pressure; τ is the stress tensor; x is the Cartesian coordinates; G_k is the generation of turbulent kinetic energy due to the mean velocity gradients; G_ω is the generation of ω; Γ_k is the effective diffusivity of k; Γ_ω is the effective diffusivity of ω; Y_k and Y_ω represent the dissipation of k and ω due to turbulence, respectively; D_ω is the cross-diffusion term; S_k and S_ω are user-defined source terms.

The inlet employs a velocity-inflow boundary condition (Velocity-inlet), simulating a Class B wind field in the calculations, represented by an exponential law for the average wind profile:

$$U(z) = U_{10}\left(\frac{z}{10}\right)^{\alpha} \tag{11}$$

where U_{10} is the average inflow wind speed at a height of 10 m, z represents the height above ground, and α is the ground roughness index. According to China's "Load Code for the Design of Building Structures" (GB50009-2012) [31], the α value for Class B wind fields is 0.15.

The turbulent kinetic energy and dissipation rate at the inflow plane are expressed as follows:

$$k(z) = \frac{3}{2} \cdot [U(z) \cdot I_u(z)]^2 \tag{12}$$

$$\varepsilon(z) = C_\mu^{3/4} \cdot \frac{k^{2/3}(z)}{K \cdot z} \tag{13}$$

where C_μ is the model constant, valued at 0.09; K is the Kármán constant, valued at 0.42; $I_{\mathrm{u}}(z)$ is the turbulent intensity of the incoming flow at height z, expressed as suggested in China's "Load Code for the Design of Building Structures" (GB50009-2012) [31]:

$$I_u(z) = I_{10} \cdot \left(\frac{z}{10}\right)^{-\alpha} \tag{14}$$

where the class B wind field I_{10} = 0.14.

The outlet employed a free outflow boundary condition (Outflow), while the lateral and top boundaries of the flow field used a free slip wall boundary condition (Free Slip Wall); all other boundaries were subjected to a no-slip wall boundary condition (No Slip Wall).

2.4. Operational Conditions

The total antenna arrangement number on the telecommunication tower ranges from 1 to 18, with the antenna arrangement layers being one to three. When each layer has an arrangement of one, three, or six antennas, the antennas are uniformly arranged on each layer, as shown in Figures 5–7. When each layer has an arrangement of two, four, or five antennas, the antennas are non-uniformly arranged on each layer, as shown in Figures 8–10. Since the antennas are symmetrically arranged, the study calculated the wind load on the structure of the telecommunication tower under all wind directions from 0° to 180°, with an angle increment of 30°, considering the influence of the antenna arrangement number, arrangement form, and arrangement layers.

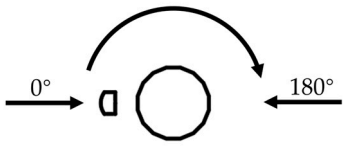

Figure 5. Arrangement form when 1 antenna is deployed.

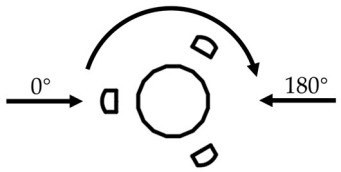

Figure 6. Arrangement form when 3 antennas are deployed.

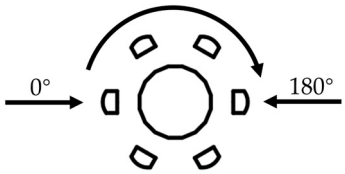

Figure 7. Arrangement form when 6 antennas are deployed.

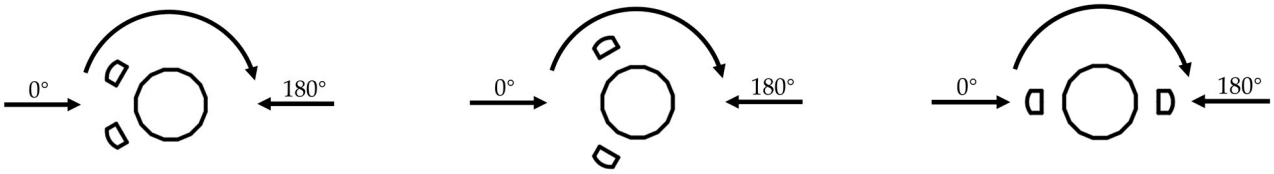

(**a**) (**b**) (**c**)

Figure 8. Arrangement form when 2 antennas are deployed. (**a**) Form 1. (**b**) Form 2. (**c**) Form 3.

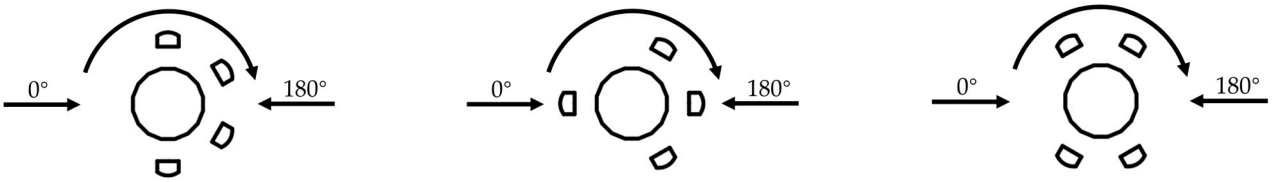

(**a**) (**b**) (**c**)

Figure 9. Arrangement form when 4 antennas are deployed. (**a**) Form 1. (**b**) Form 2. (**c**) Form 3.

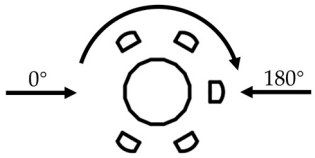

Figure 10. Arrangement form when 5 antennas are deployed.

3. Numerical Calculation Results and Analysis

3.1. Comparison of Numerical Simulation Results with Wind Tunnel Test Results

To verify the accuracy and reliability of the numerical simulations conducted in this study, we compared the simulation results with wind tunnel test results reported in

the existing literature [14]. The antenna shapes and tower cylinder shapes used in the referenced literature and in this study are quite similar, and the corresponding antenna arrangement forms are essentially the same. Differences in details have a minor impact on the overall wind load. Hence, the aerodynamic coefficients obtained in the referenced literature and in this study are expected to be close. Table 3 presents the comparison of the drag coefficients of the telecommunication tower obtained from wind tunnel tests and numerical simulations when a single layer of three antennas is used. It can be seen that the values of the drag coefficients obtained by both methods are very close, and their variation trends with the wind direction are also consistent. This not only proves the accuracy of the numerical simulation method used in this study but also enhances the credibility of the research findings.

Table 3. Comparison of the drag coefficients of the telecommunication tower obtained from wind tunnel tests and numerical simulations.

Research Method	C_D at 0° Wind Direction	C_D at 30° Wind Direction	C_D at 60° Wind Direction
Numerical simulation	0.8241	0.8254	0.7729
Wind tunnel test	0.8289	0.8565	0.7481

3.2. Impact of Antenna Arrangement Number and Arrangement Form on the Wind Load of Telecommunication Towers

When only one layer of telecommunication antennas is arranged on the tower, it is possible to have one to six antennas in this single layer. When arranging one, three, five, or six antennas, there is only one arrangement form. However, when arranging two or four antennas, there are multiple arrangement forms.

When arranging two antennas, there are three forms, as shown in Figure 8. The wind load on the telecommunication tower as a function of the wind direction is shown in Figure 11. Figure 11a,b illustrate the drag coefficient and the windward base overturning moment coefficient of the telecommunication tower, respectively, while Figure 11c,d present the lateral force coefficient and the crosswind base overturning moment coefficient, respectively. The drag coefficient and lateral force coefficient were combined to derive the overturning force coefficient for the telecommunication tower, as demonstrated in Figure 11e. Similarly, the windward and crosswind base overturning moment coefficients were combined to yield the overturning moment coefficient for the telecommunication tower, as shown in Figure 11f. From Figure 11, it is evident that the lateral force coefficient and the crosswind base overturning moment coefficient are significantly smaller compared to the drag coefficient and the windward base overturning moment coefficient. Consequently, after combining, the values of the drag coefficient and the windward base overturning moment coefficient are very close to those of the overturning force coefficient and the overturning moment coefficient.

As shown in Figure 11, it is evident that the arrangement form of the antennas significantly affects the wind load on the telecommunication tower. The poorer the symmetry after antenna arrangement, the greater the values of the lateral force coefficient and crosswind base overturning moment coefficient of the telecommunication tower. The distribution curves of the tower's overturning force coefficient and overturning moment coefficient generally follow a similar trend. When two antennas are in arrangement form 1, both the overturning force coefficient and overturning moment coefficient of the tower exhibit a sawtooth pattern as the wind direction changes. When two antennas are in arrangement form 2, from 0° to 120° wind directions, the fluctuations in the overturning force coefficient and overturning moment coefficient curves are relatively mild, but they increase rapidly from 120° to 180°, reaching their maximum values at 180°. Compared to the bare tower condition without antennas, the overturning force coefficient and the overturning moment coefficient increased by 14.7% and 26.4%, respectively. When two antennas are in arrangement form 3, the tower's overturning force coefficient and overturning moment

coefficient reach their maximum values at wind directions of 60° and 120°, and for most wind directions, both coefficients are higher than those of the other two arrangement forms.

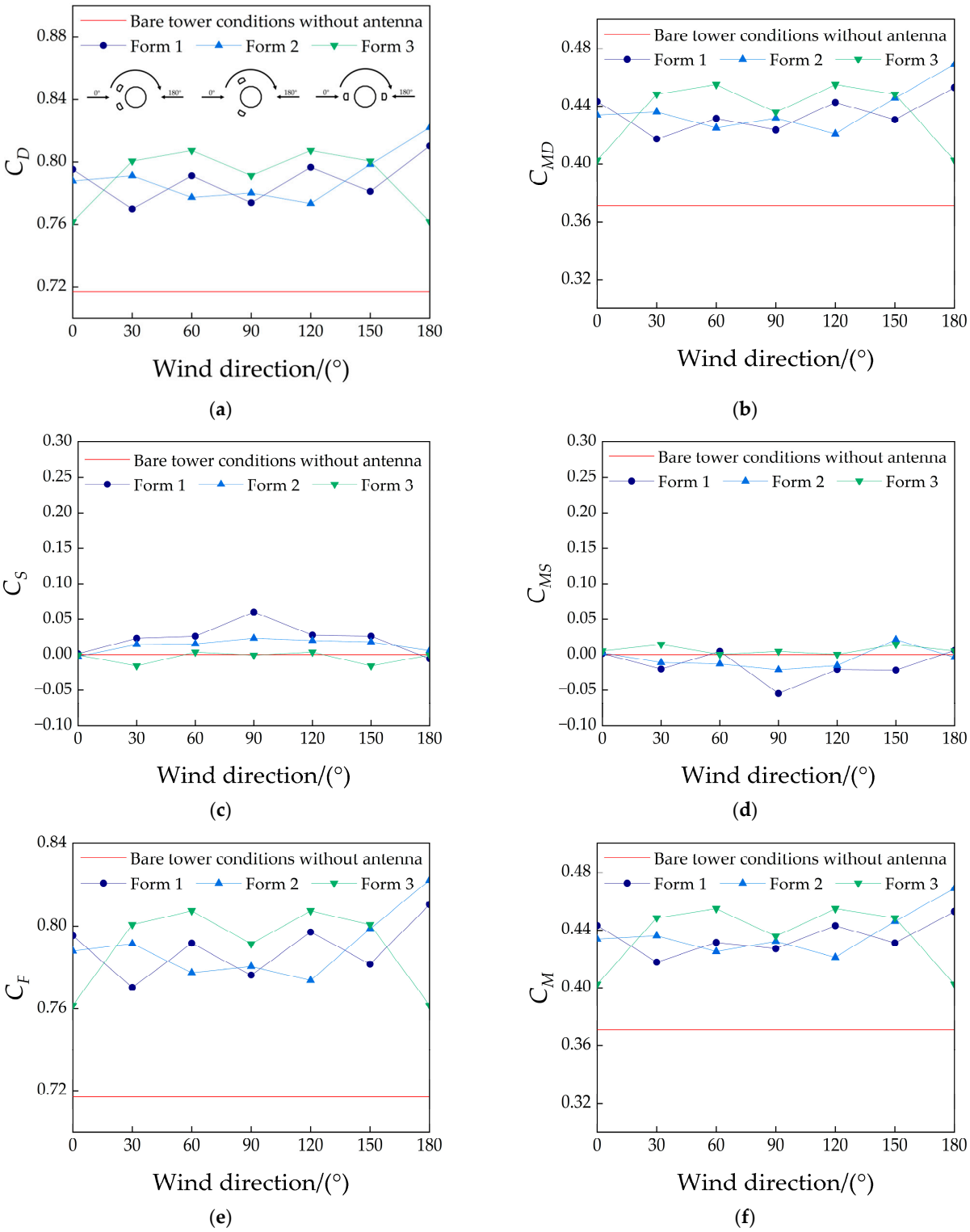

Figure 11. Variation curve of wind load on the telecommunication tower with wind direction when 2 antennas are arranged. (**a**) Drag coefficient. (**b**) Windward base overturning moment coefficient. (**c**) Lateral force coefficient. (**d**) Crosswind base overturning moment coefficient. (**e**) Overturning force coefficient. (**f**) Overturning moment coefficient.

Figure 12 shows the flow fields at the mid-height cross-section of the antennas for three different arrangement forms when two antennas are arranged in a single layer. When the circular end of the antenna faces the wind, the wake region is small, resulting in a lower overturning force coefficient; when the flat end of the antenna faces the wind, the wake region noticeably enlarges, causing an increase in the overturning force coefficient.

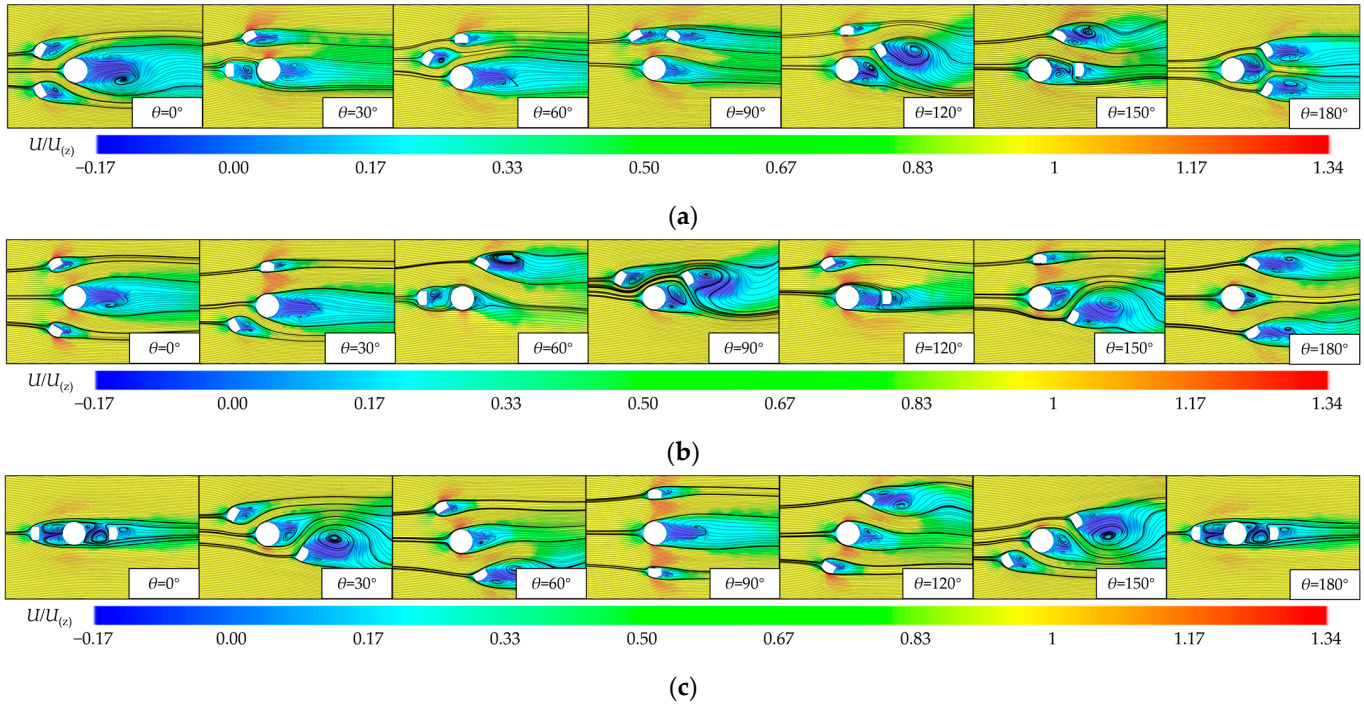

Figure 12. Velocity contour and streamline diagram at the mid-height cross-section of the antennas when 2 antennas are arranged. (**a**) Form 1. (**b**) Form 2. (**c**) Form 3.

When two antennas are arranged in form 1, as shown in Figure 12a, within the 0° to 60° wind direction range, both antennas are located upstream of the tower cylinder, and with their circular ends facing the wind. The tower cylinder disrupts the wake and vortex formation area of the antennas. The upstream antenna significantly obstructs the inflow toward the tower cylinder, and its wake alters the characteristics of the flow, impacting the tower cylinder. At a 30° wind direction, relative to the inflow direction, one antenna is directly in front of the tower cylinder with a small gap, causing the antenna's separation shear layer to attach to the downstream tower cylinder, significantly reducing the flow velocity in the gap and, thus, decreasing the overturning force coefficient on the telecommunication tower. At a 90° wind direction, relative to the inflow direction, one antenna is directly in front of the other, and due to the small gap, they are also in a shear layer reattachment state, resulting in a reduction of the overturning force coefficient on the tower. In the 120° to 180° wind direction range, the tower cylinder is upstream of the antennas, and with the flat end of the antennas facing the wind, the wake region enlarges significantly, leading to a greater overturning force coefficient. At a 150° wind direction, relative to the inflow direction, the tower cylinder is directly in front of one antenna, causing the tower cylinder's separation shear layer to attach to the surface of the downstream antenna, resulting in a reduction of the overturning force coefficient on the tower. This is why the overturning force coefficient of the telecommunication tower varies in a sawtooth pattern with the wind direction. At a 180° wind direction, the presence of the two antennas causes the wall boundary layer separation point on the tower cylinder to move forward, increasing the overturning force coefficient; at the same time, the large windward angles of the flat ends of the antennas enlarge the wake region, further

increasing the overturning force coefficient, thus significantly enhancing the overturning force coefficient on the telecommunication tower at a 180° wind direction.

When two antennas are arranged in form 2, as shown in Figure 12b, within the 60° to 120° wind direction range, the blocking effect between the antennas and the tower cylinder, and between the antennas themselves, is significant, reducing the overturning force coefficient on the telecommunication tower. At a 180° wind direction, the interference effect between the antennas and the tower cylinder, and between the antennas themselves, is weaker, and with the flat end of the antennas facing the wind, the wake region enlarges significantly, resulting in the highest overturning force coefficient on the telecommunication tower at this wind direction.

When two antennas are arranged in form 3, as shown in Figure 12c, at the 0° and 180° wind directions, relative to the inflow direction, the two antennas and the tower cylinder are in a serial arrangement, resulting in the strongest blocking effect among these three elements, significantly reducing the overturning force coefficient on the telecommunication tower. In the 30° to 150° wind direction range, compared to forms 1 and 2, the interference effect between the antennas and the tower cylinder, and between the antennas in form 3, is significantly weakened, thus the overturning force coefficient on the tower is higher than the other two arrangement forms.

For an arrangement of four antennas, there are three arrangement forms, as shown in Figure 9, and the variation curve of the wind load on the telecommunication tower with the wind direction is shown in Figure 13. When four antennas are in arrangement form 1, the tower's overturning force coefficient and overturning moment coefficient are most sensitive to changes in the wind direction. At a 90° wind direction, both the overturning force coefficient and overturning moment coefficient of the tower significantly decrease, reaching their lowest values. When four antennas are in arrangement form 2, the tower's overturning force coefficient and overturning moment coefficient significantly decrease at wind directions of 60° and 180°. When four antennas are in arrangement form 3, the variation curves of the tower's overturning force coefficient and overturning moment coefficient with wind direction are relatively gentle, showing insensitivity to changes in the wind direction.

Figure 14 shows the flow fields at the mid-height cross-section of the antennas for three different arrangement forms when four antennas are arranged in a single layer. As shown in Figure 14, with four antennas in arrangement form 1, at a 0° wind direction, the interference effects between the antennas and the tower cylinder, and between the antennas themselves, are weaker. Moreover, all four antennas have their flat ends facing the wind, significantly enlarging the wake region, which results in the highest overturning force coefficient on the telecommunication tower; at a 90° wind direction, relative to the inflow direction, two of the antennas and the tower cylinder are in a serial arrangement, and the remaining two antennas are also serially arranged, resulting in the strongest blocking effect and significantly reducing the overturning force coefficient on the telecommunication tower. When four antennas are in arrangement form 2, at the 0° and 180° wind directions, relative to the inflow direction, there are two antennas and the tower cylinder in a serial arrangement, but at the 180° wind direction, the remaining two antennas face the wind with their circular ends, significantly reducing the wake region and, thus, lowering the overturning force coefficient of the tower. At the 60° and 120° wind directions, there is one antenna and the tower cylinder in a serial arrangement, and another two antennas are also serially arranged, but at the 60° wind direction, one antenna is completely in the wake region of the tower cylinder, and the fourth antenna is facing the wind with its circular end, also significantly reducing the wake region, resulting in a decrease in the overturning force coefficient of the tower. When four antennas are in arrangement form 3, due to the better uniformity of the four antennas, the flow field around them changes less with wind direction, making the overturning force coefficient on the tower less sensitive to changes in the wind direction.

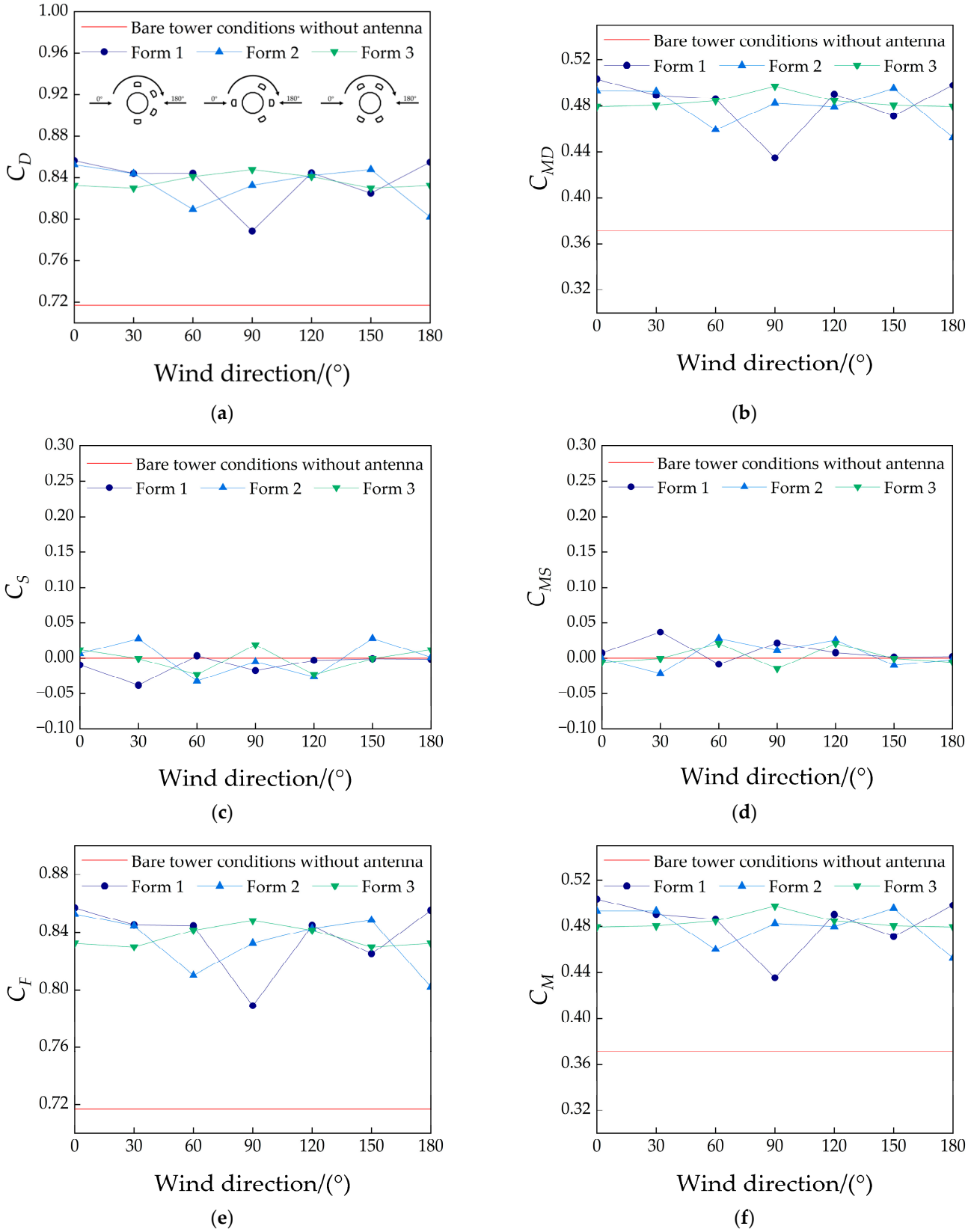

Figure 13. Variation curve of wind load on the telecommunication tower with wind direction when 4 antennas are arranged. (**a**) Drag coefficient. (**b**) Windward base overturning moment coefficient. (**c**) Lateral force coefficient. (**d**) Crosswind base overturning moment coefficient. (**e**) Overturning force coefficient. (**f**) Overturning moment coefficient.

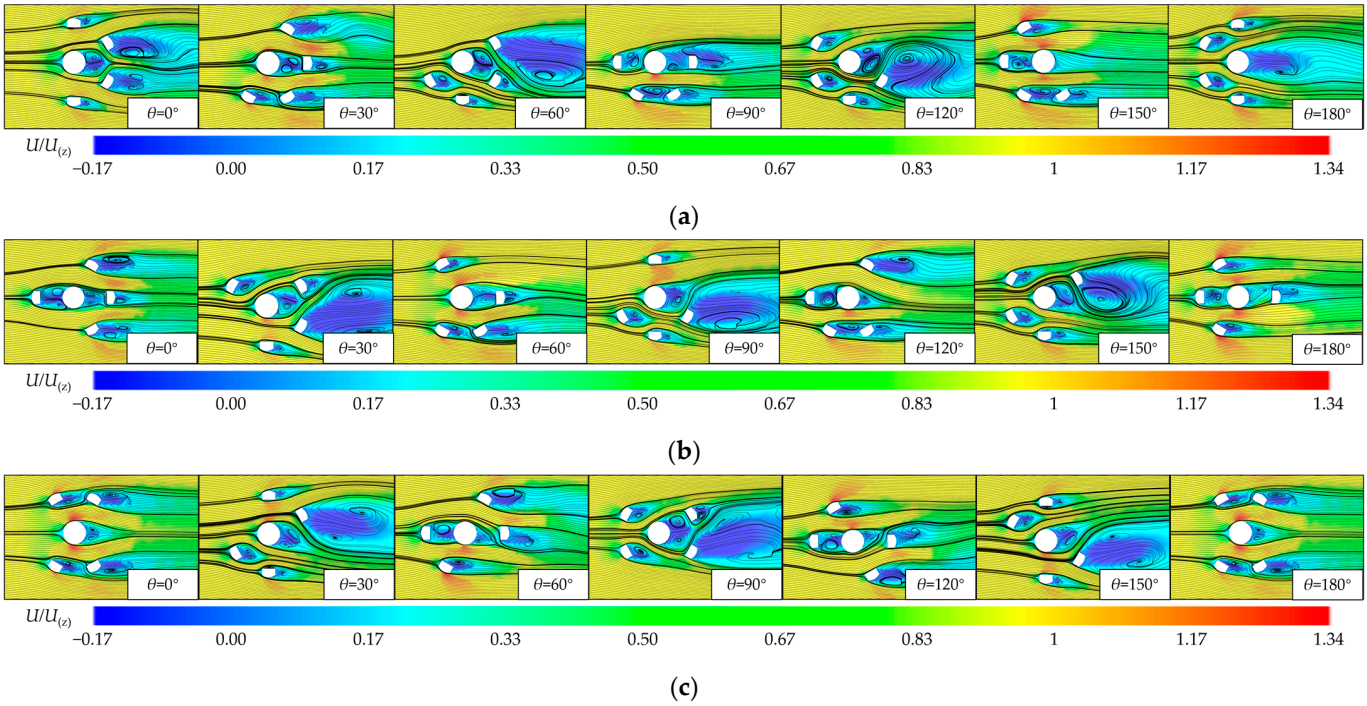

Figure 14. Velocity contour and streamline diagram at the mid-height cross-section of the antennas when 4 antennas are arranged. (**a**) Form 1. (**b**) Form 2. (**c**) Form 3.

Figure 15 shows in detail the variation of the wind load on the telecommunication tower with the antenna arrangement number for a single layer arrangement under different wind directions, where the cases with two and four antennas display the maximum wind load coefficient values for different arrangement forms.

From Figure 15, it can be seen that the values of the drag coefficient and the windward base overturning moment coefficient are always very close to those of the overturning force coefficient and the overturning moment coefficient. The lateral force coefficient and the crosswind base overturning moment coefficient of the telecommunication tower vary with the antenna arrangement number in a similar pattern and are very small in value, showing a trend of initially increasing and then decreasing as the antenna arrangement number increases. The maximum value is reached when two antennas are arranged at a 90° wind direction.

It is also clear that the sensitivity of the telecommunication tower's overturning force coefficient to the wind direction varies with different antenna arrangement numbers. When a single antenna is used in the arrangement, the overturning force coefficient of the tower changes slightly within the 30° to 150° wind direction range and significantly decreases at the 0° and 180° wind directions, approaching the bare tower condition without antennas. When three antennas are used in the arrangement, the tower's overturning force coefficient significantly decreases at the 60° and 180° wind directions, with the overturning force coefficient values being nearly equal at other wind directions. When five and six antennas are used in the arrangement, the variation curves of the tower's overturning force coefficient with the wind direction are approximately sawtooth-shaped, but with five antennas, the coefficient is more sensitive to the wind direction, with a larger range of variation. Overall, when a single layer of antennas is arranged on the tower, the overturning force coefficient tends to increase with the antenna arrangement number, but the extent of the increase gradually diminishes as the antenna arrangement number increases. The pattern of change in the overturning moment coefficient of the telecommunication tower with the antenna arrangement number is basically consistent with that of the overturning force coefficient, but with an increase in the antenna arrangement number, the magnitude of increase in the overturning moment coefficient is about twice that of the overturning force coefficient.

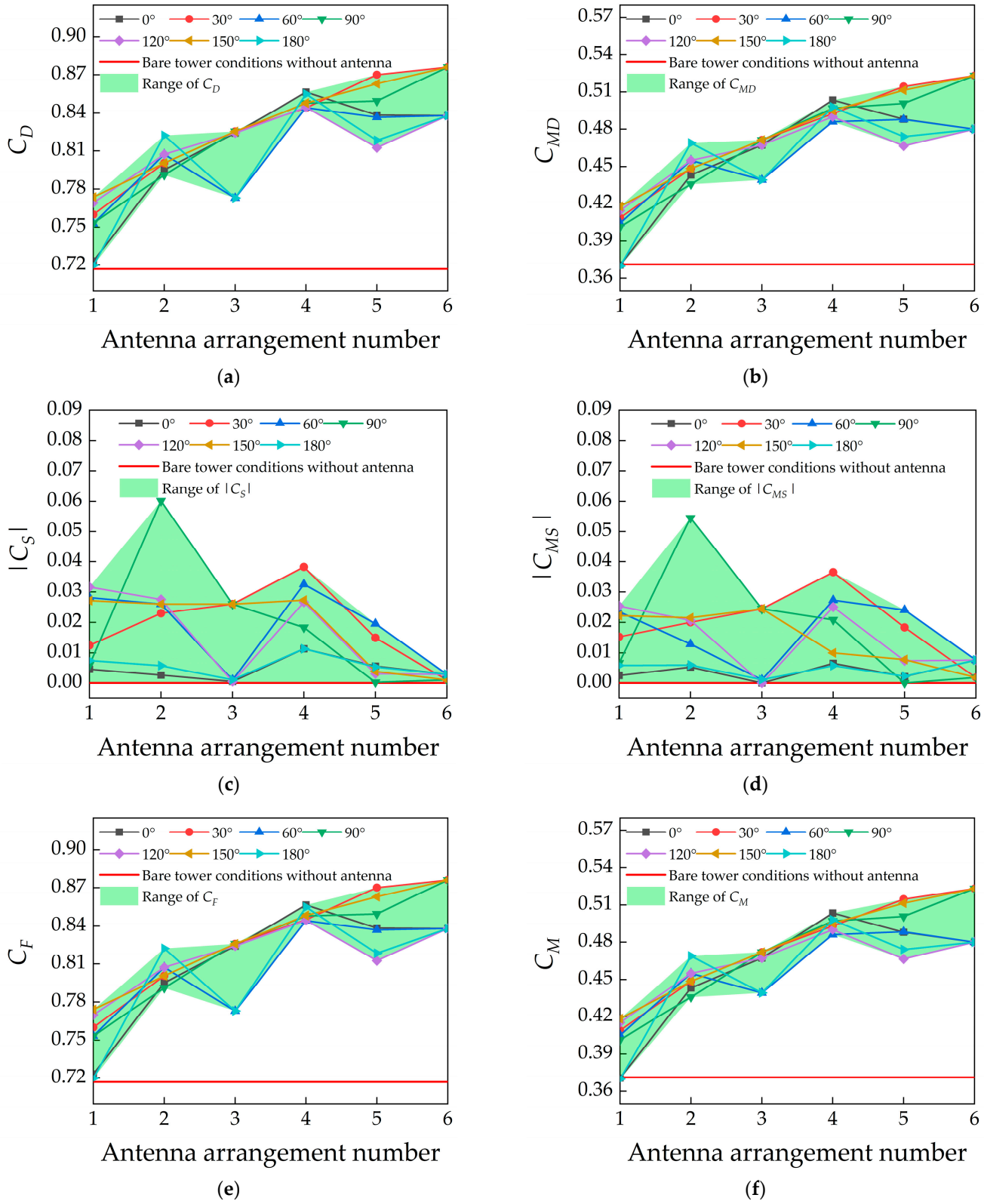

Figure 15. Impact of single-layer antenna arrangement on the wind load of telecommunication towers. (**a**) Drag coefficient. (**b**) Windward base overturning moment coefficient. (**c**) Lateral force coefficient. (**d**) Crosswind base overturning moment coefficient. (**e**) Overturning force coefficient. (**f**) Overturning moment coefficient.

3.3. Impact of the Antenna Arrangement Layers on the Wind Load of Telecommunication Towers

When two or three layers of antennas are arranged on the telecommunication tower, each layer can accommodate three to six antennas, with the total antenna arrangement number being 6 to 18.

Through a comparison with Section 3.2, it was found that the rate of increase in the wind load with the antenna arrangement layers is significantly greater than with the antenna arrangement number. Figures 16–19 illustrate the flow fields around the telecommunication tower under the arrangement forms associated with the maximum wind load when one layer of antennas with six antennas per layer is used, two layers with three antennas per layer, two layers with six antennas per layer, and three layers with four antennas per layer, respectively. When the total antenna arrangement number is the same, as shown in Figures 16–19, it can be seen that the interference effect between the antennas arranged on different layers is weak. Increasing the antenna arrangement layers significantly enlarges the wake region, thereby substantially increasing the overturning force coefficient. Therefore, to reduce the wind load, it is advisable in practical engineering applications to increase the antenna arrangement number per layer, thereby reducing the antenna arrangement layers.

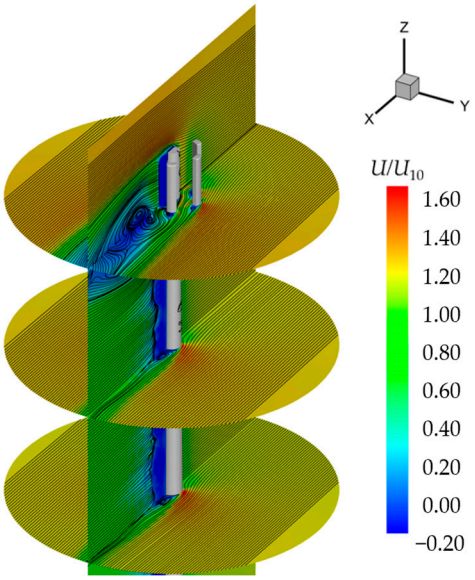

Figure 16. Flow field around the telecommunication tower with 1 layer of antennas, 6 antennas per layer, at a wind direction of 30°.

The distribution pattern of wind loads on the telecommunication tower is shown in Figures 20–25, where the values for the case of four antennas per layer represent the maximum wind load coefficient values among the three arrangement forms. By comparing Figures 20–25, it can be observed that when arranging multiple layers of antennas, the lateral force coefficient and the crosswind base overturning moment coefficient remain significantly smaller compared to the drag coefficient and the windward base overturning moment coefficient. Therefore, the values of the drag coefficient and the windward base overturning moment coefficient are very close to those of the overturning force coefficient and the overturning moment coefficient.

The absolute values of the lateral force coefficient and the crosswind base overturning moment coefficient of the telecommunication tower, as they vary with the antenna arrangement layers and wind direction, are shown in Figures 22 and 23. Compared to the drag coefficient and windward base overturning moment coefficient, the lateral force coefficient and crosswind base overturning moment coefficient of the telecommunication tower are more sensitive to changes in the wind direction. They exhibit a greater range of growth

rates with the increase in the antenna arrangement layers. As the symmetry of the antennas relative to the inflow wind direction improves, the values of the telecommunication tower's lateral force coefficient and crosswind base overturning moment coefficient become lower. When arranging four antennas per layer, at wind directions of 0° and 180°, the symmetry is optimal, resulting in the smallest lateral force coefficient and crosswind base overturning moment coefficient at these wind directions, showing insensitivity to the increase in antenna arrangement layers. The absolute values of the tower's lateral force coefficient and crosswind base overturning moment coefficient reach 0 to 0.115 and 0 to 0.093, respectively.

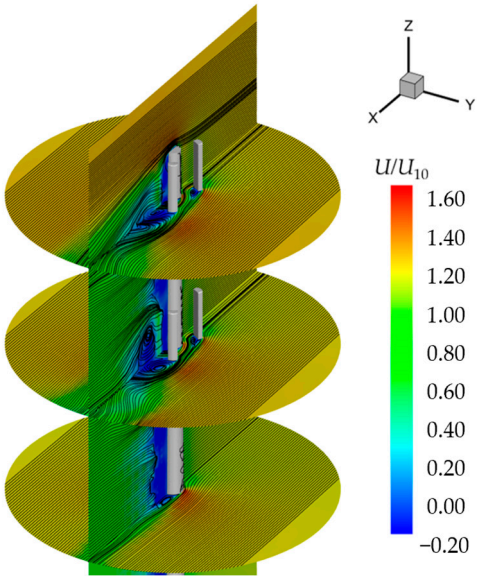

Figure 17. Flow field around the telecommunication tower with 2 layers of antennas, 3 antennas per layer, at a wind direction of 30°.

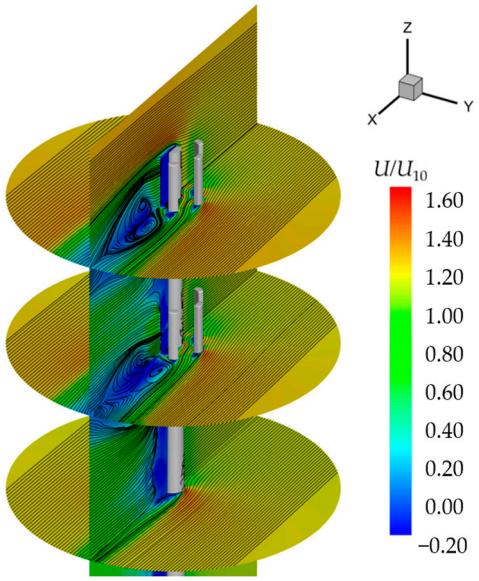

Figure 18. Flow field around the telecommunication tower with 2 layers of antennas, 6 antennas per layer, at a wind direction of 30°.

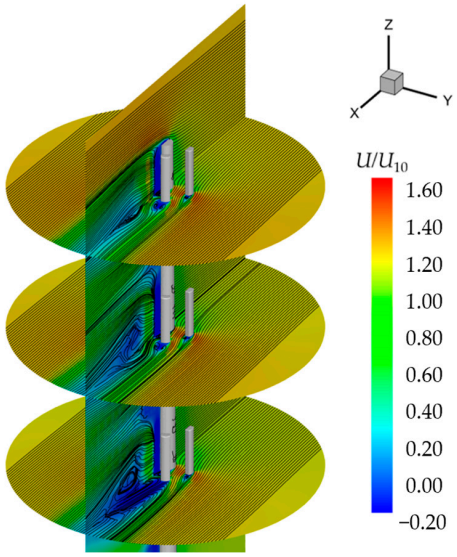

Figure 19. Flow field around the telecommunication tower with 3 layers of antennas, 4 antennas per layer arranged in form 1, at a wind direction of 0°.

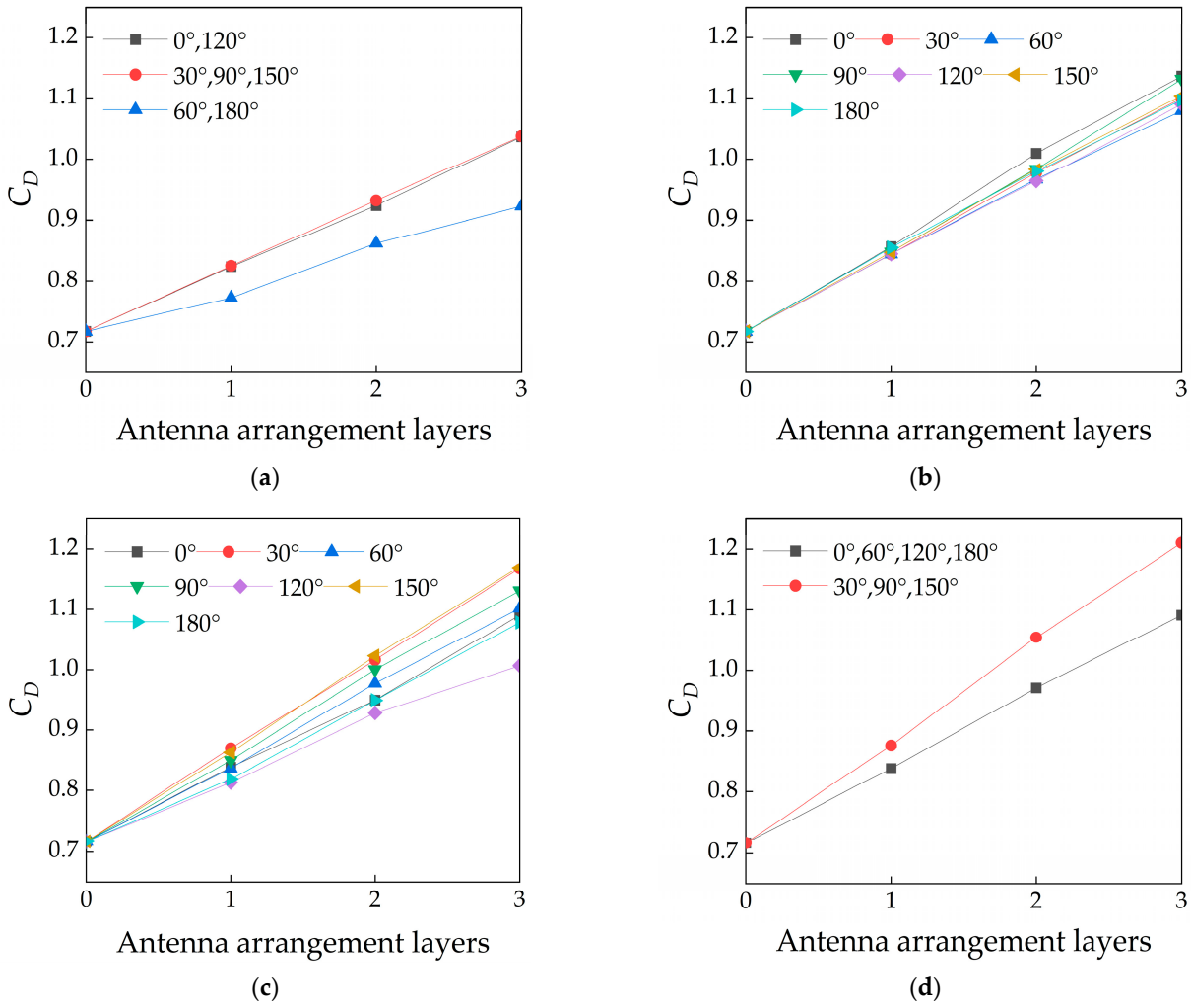

Figure 20. Variation curve of drag coefficient of telecommunication tower with antenna arrangement layers. (**a**) Three antennas per layer. (**b**) Four antennas per layer. (**c**) Five antennas per layer. (**d**) Six antennas per layer.

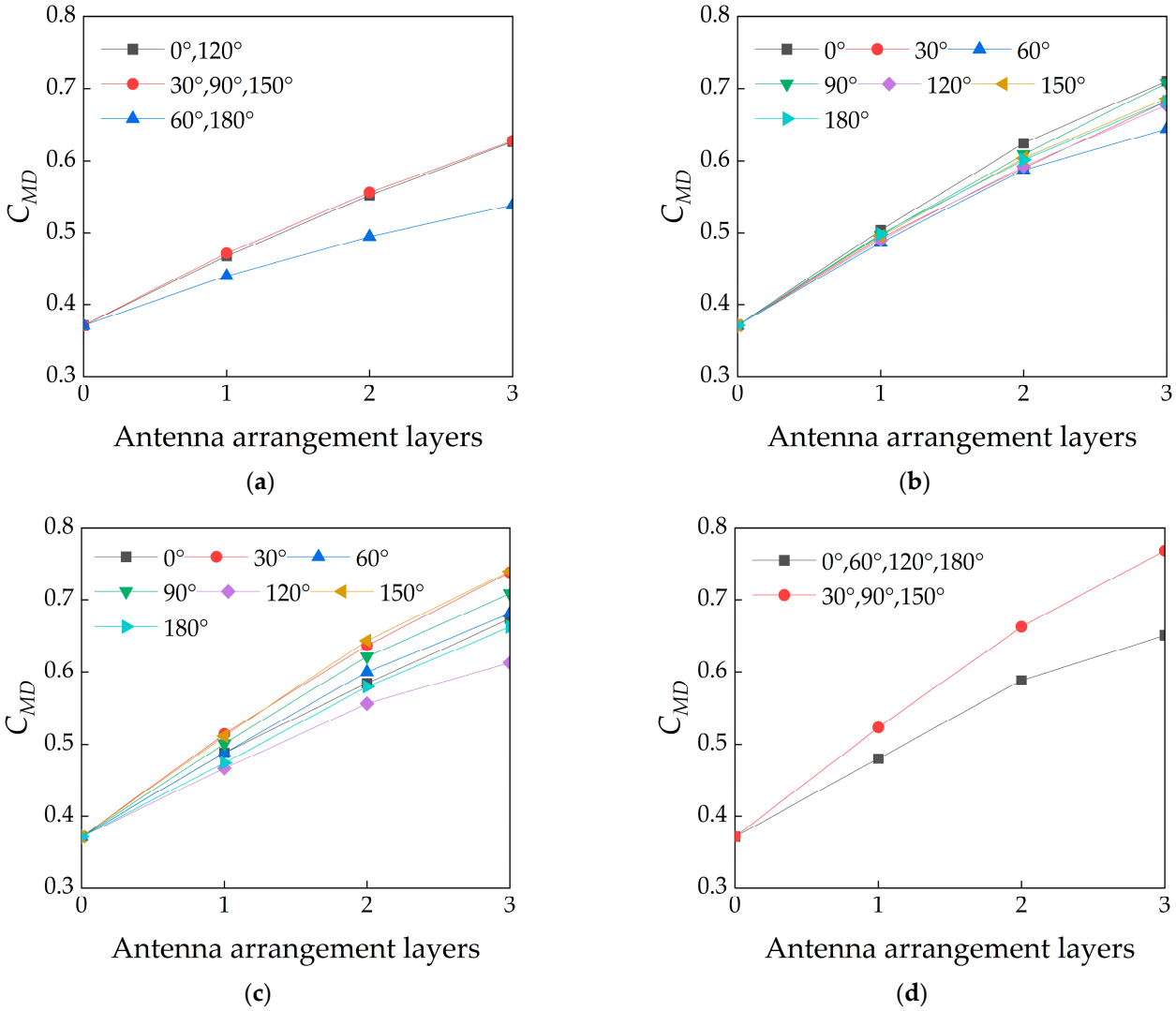

Figure 21. Variation curve of windward base overturning moment coefficient of telecommunication tower with antenna arrangement layers. (**a**) Three antennas per layer. (**b**) Four antennas per layer. (**c**) Five antennas per layer. (**d**) Six antennas per layer.

Moreover, as the antenna arrangement number per layer increases, the growth rate of the telecommunication tower's lateral force coefficient and the crosswind base overturning moment coefficient with the antenna arrangement layers initially rises and then falls. The maximum growth rate occurs when there are four antennas per layer, and the minimum growth rate is observed with six antennas per layer.

As shown in Figure 24, when the antenna arrangement number per layer is the same, the overturning force coefficient of the telecommunication tower approximately linearly increases with the increase in antenna arrangement layers. Moreover, as the antenna arrangement number per layer increases, the growth rate of the tower's overturning force coefficient with the antenna arrangement layers also gradually increases.

When three antennas are arranged per layer, the rate of increase in the telecommunication tower's overturning force coefficient with the antenna arrangement layers ranges from 7.0% to 15.2%. At the 0°, 30°, 90°, 120°, and 150° wind directions, the rate of increase in the telecommunication tower's overturning force coefficient with the antenna arrangement layers is very close, significantly higher than at the 60° and 180° wind directions, i.e., approximately 1.5 times higher; when four antennas are arranged per layer, the rate of increase ranges from 11.7% to 19.5%; with five antennas per layer, the range is 8.5% to 21.4%, which is the most sensitive to the wind direction, reaching the maximum values at

either the 30° or 150° wind direction; and with six antennas per layer, the rate of increase in the telecommunication tower's overturning force coefficient ranges from 12.4% to 22.2%. At the 30°, 90°, and 150° wind directions, the rate of increase in the telecommunication tower's overturning force coefficient with the antenna arrangement layers is very close, significantly higher than at the 0°, 60°, 120°, and 180° wind directions, i.e., approximately 1.3 times higher.

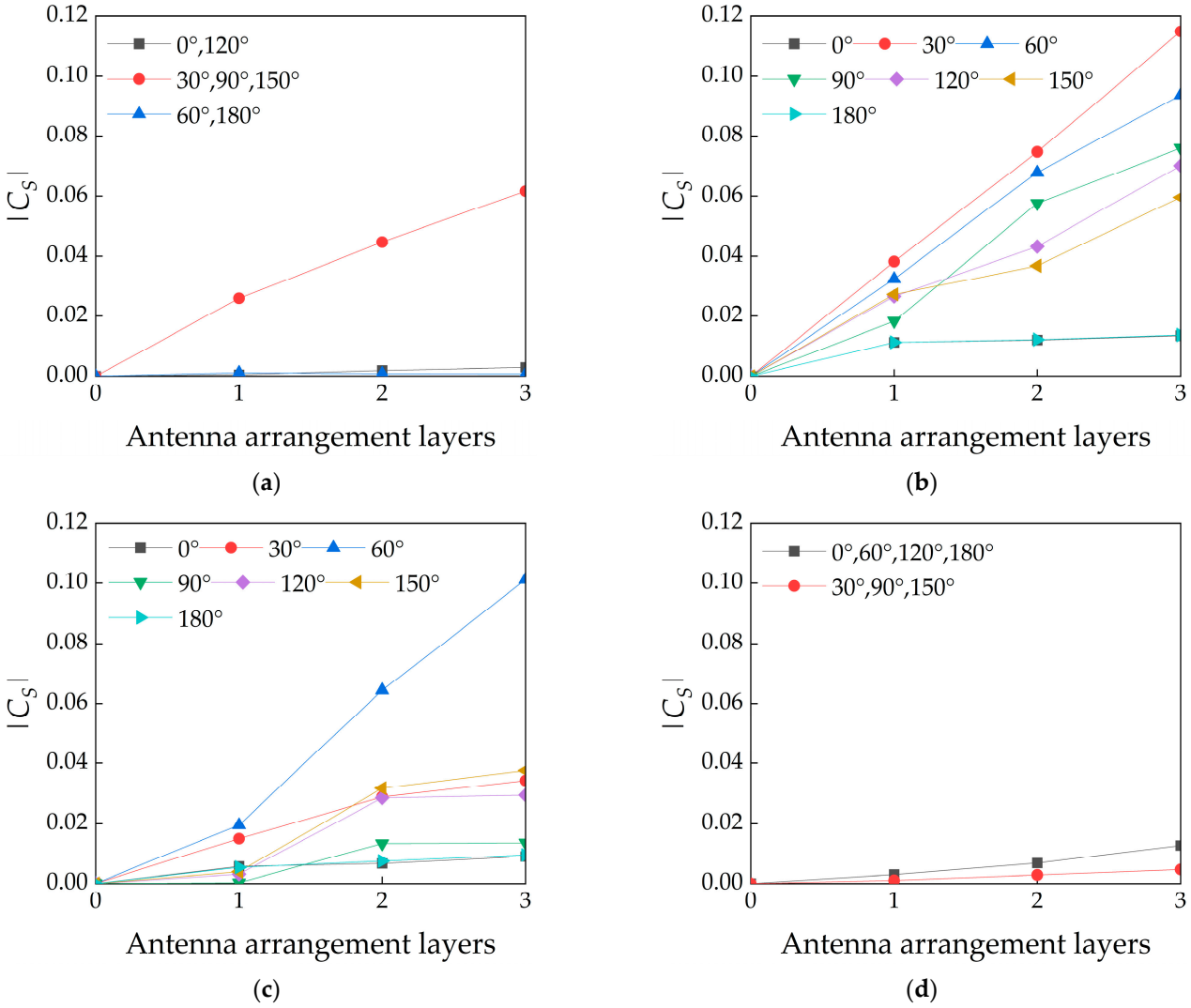

Figure 22. Variation curve of lateral force coefficient of telecommunication tower with antenna arrangement layers. (**a**) Three antennas per layer. (**b**) Four antennas per layer. (**c**) Five antennas per layer. (**d**) Six antennas per layer.

Figure 25 presents the variation curve of the overturning moment coefficient of the telecommunication tower in relation to the antenna arrangement layers and wind direction. From the figure, it is evident that when the antenna arrangement number per layer remains constant, the overturning moment coefficient of the telecommunication tower exhibits a nonlinear increase with additional antenna arrangement layers, which significantly differs from the trend observed in the overturning force coefficient. Moreover, as the antenna arrangement number per layer increases, the rate of increase in the telecommunication tower's overturning moment coefficient with antenna arrangement layers also gradually increases, and is significantly greater than the rate of increase in the overturning force coefficient with antenna arrangement layers. As demonstrated, when three to six antennas are arranged per layer, the range of the growth rate of the overturning moment coefficient

with antenna arrangement layers gradually elevates, specifically to 8.8% to 27.2%, 9.8% to 35.7%, 10.2% to 38.7%, and 10.8% to 41.0%, which is markedly higher than the growth rate of the overturning force coefficient with antenna arrangement layers.

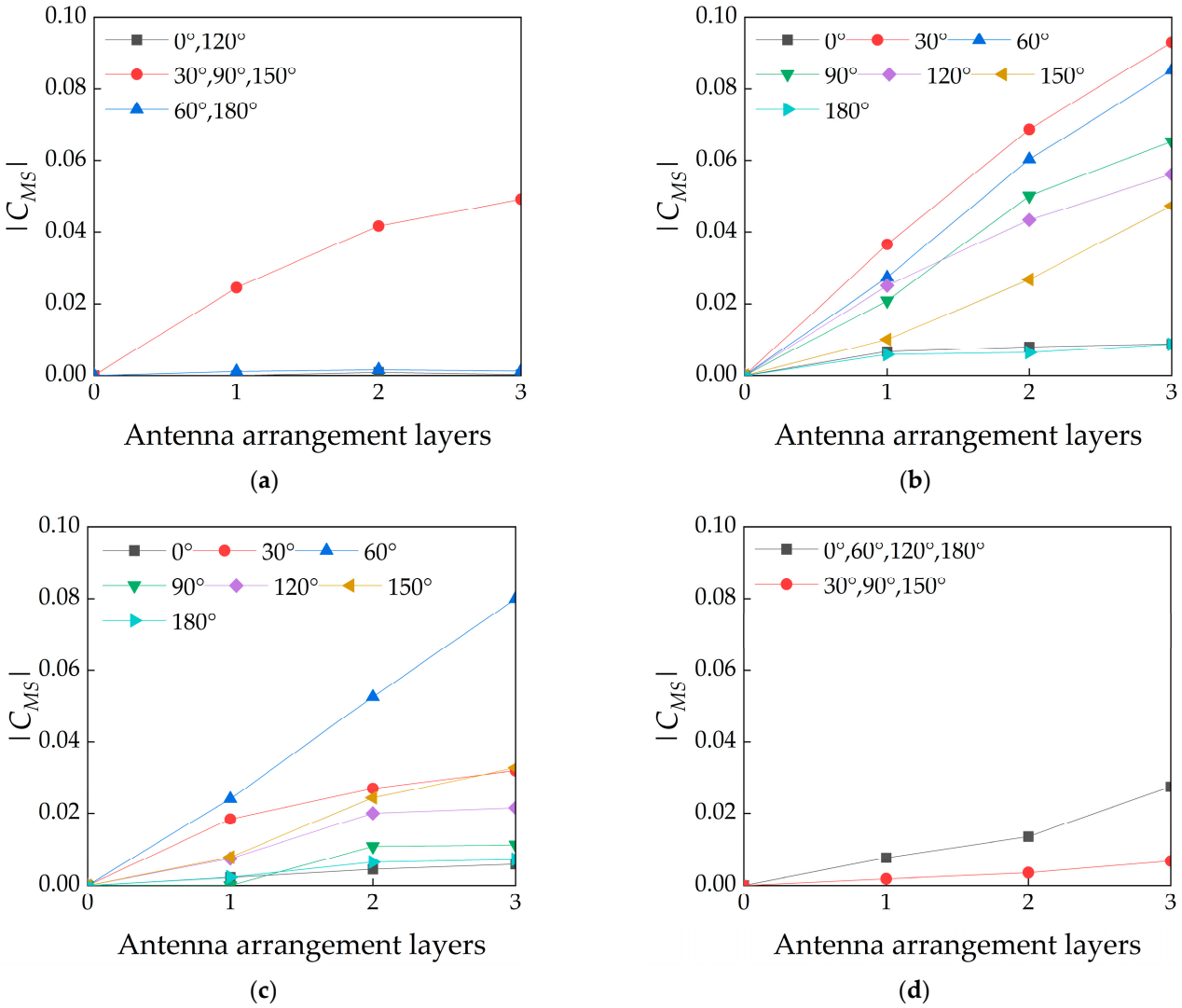

Figure 23. Variation curve of crosswind base overturning moment coefficient of telecommunication tower with antenna arrangement layers. (**a**) Three antennas per layer. (**b**) Four antennas per layer. (**c**) Five antennas per layer. (**d**) Six antennas per layer.

In order to further analyze the impact of the antenna arrangement layers on the wind load of the telecommunication tower, the maximum values of wind loads for all wind directions were used to eliminate the influence of wind direction, as shown in Figure 26.

The values of the drag coefficient and the windward base overturning moment coefficient are very close to those of the overturning force coefficient and the overturning moment coefficient.

With the increase in the antenna arrangement layers, the lateral force coefficient and the crosswind base overturning moment coefficient of the telecommunication tower gradually increase. Moreover, the rate of increase in both coefficients with antenna arrangement layers is significantly influenced by the antenna arrangement number per layer, with the highest rate of increase when four antennas are arranged per layer, and the lowest when six antennas are arranged per layer.

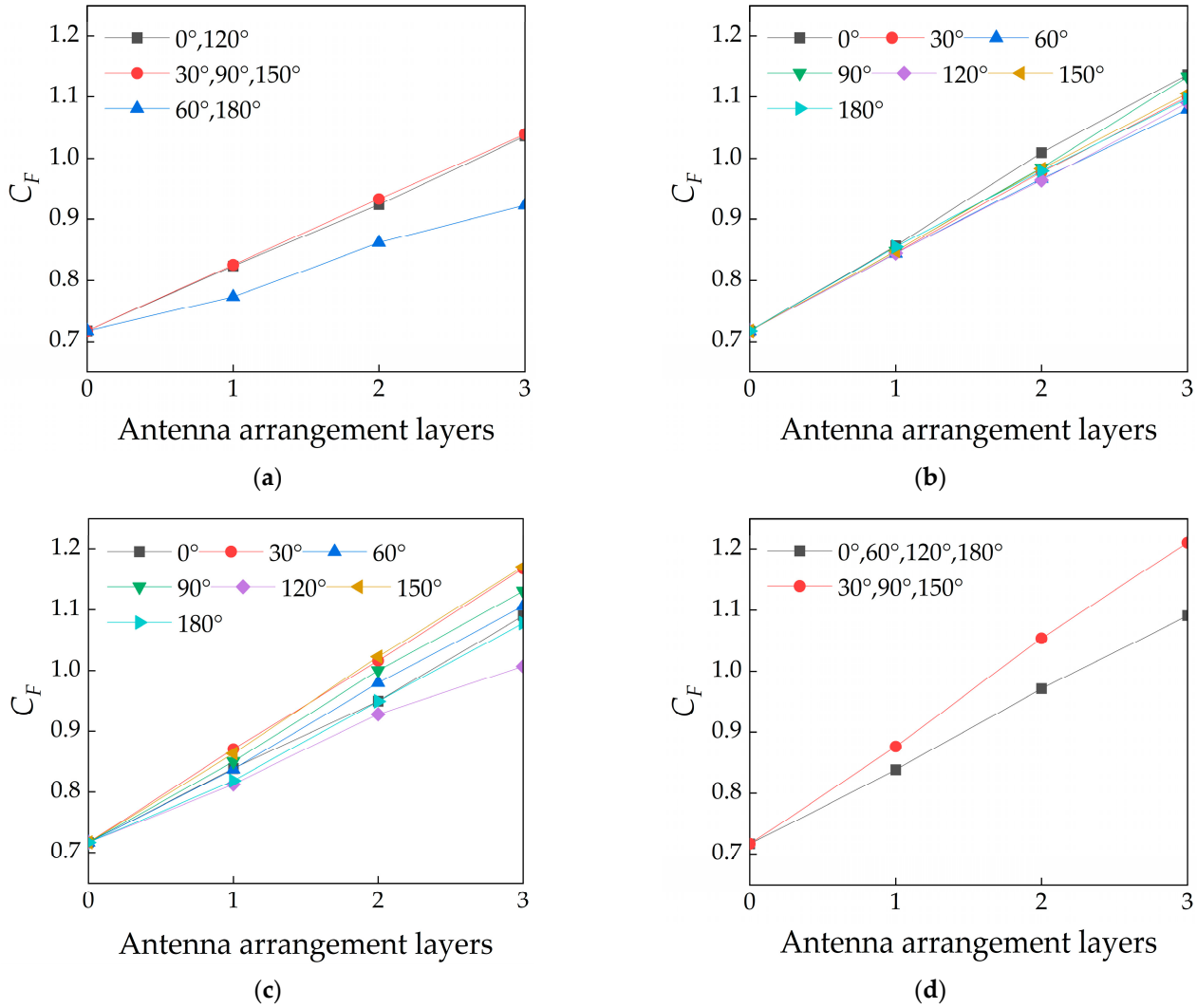

Figure 24. Variation curve of overturning force coefficient of telecommunication tower with antenna arrangement layers. (**a**) Three antennas per layer. (**b**) Four antennas per layer. (**c**) Five antennas per layer. (**d**) Six antennas per layer.

The overturning force coefficient of the telecommunication tower increases approximately linearly with the increase in antenna arrangement layers, showing good consistency. Furthermore, the greater the antenna arrangement number per layer, the higher the rate of increase in the overturning force coefficient with antenna arrangement layers. Specifically, when four antennas are arranged per layer, the growth rate of the telecommunication tower's overturning force coefficient with antenna arrangement layers is significantly higher than the case with three antennas per layer, but the difference narrows significantly compared to the cases with five or six antennas per layer.

As the antenna arrangement layers increase, the overturning moment coefficient of the tower also gradually increases, but the rate of increase gradually decreases. Similar to the overturning force coefficient, the rate of increase in the tower's overturning moment coefficient with the antenna arrangement layers is significantly higher when four antennas are arranged per layer compared to the case with three antennas per layer, but the gap narrows significantly when compared to cases with five and six antennas per layer.

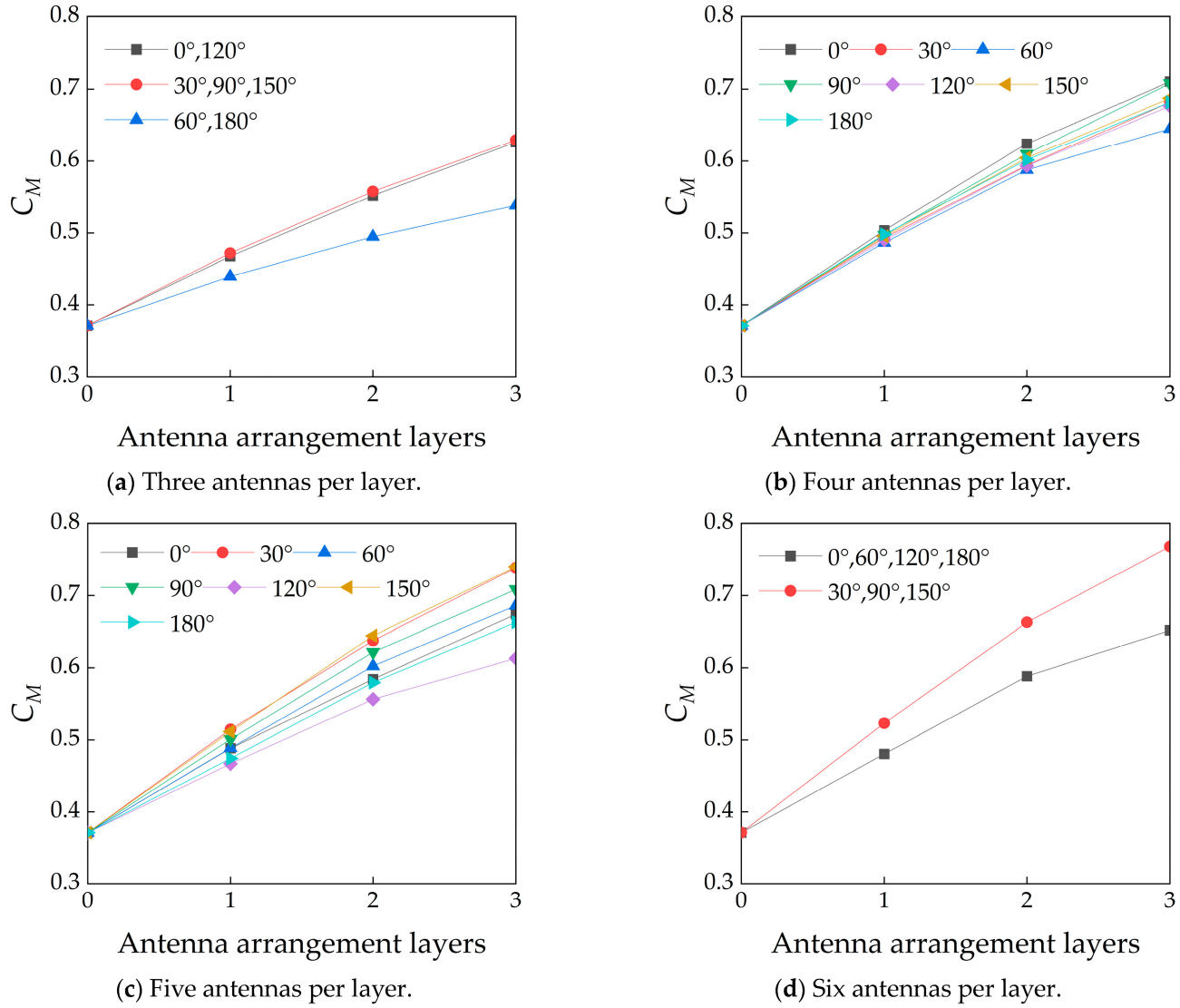

(**a**) Three antennas per layer.

(**b**) Four antennas per layer.

(**c**) Five antennas per layer.

(**d**) Six antennas per layer.

Figure 25. Variation curve of overturning moment coefficient of telecommunication tower with antenna arrangement layers. (**a**) Three antennas per layer. (**b**) Four antennas per layer. (**c**) Five antennas per layer. (**d**) Six antennas per layer.

Figure 27 shows the flow field around the telecommunication tower when six antennas are arranged per layer, with antenna arrangement layers varying from one to three. The figure reveals that the interference effect between antennas arranged on different layers is weak, which explains why the overturning force coefficient approximately exhibits a linear increase with antenna arrangement layers.

3.4. Calculation Method for Wind Load on Telecommunication Towers Considering Antenna Arrangement Parameters

Through a three-dimensional numerical simulation, the overturning force coefficient C_F and overturning moment coefficient C_M of the telecommunication tower were obtained for each condition. The maximum values of the telecommunication tower's overturning force coefficient C_{Fmax} and the overturning moment coefficient C_{Mmax} under all wind directions (α = 0° to 180°) were determined, as shown in Table 4.

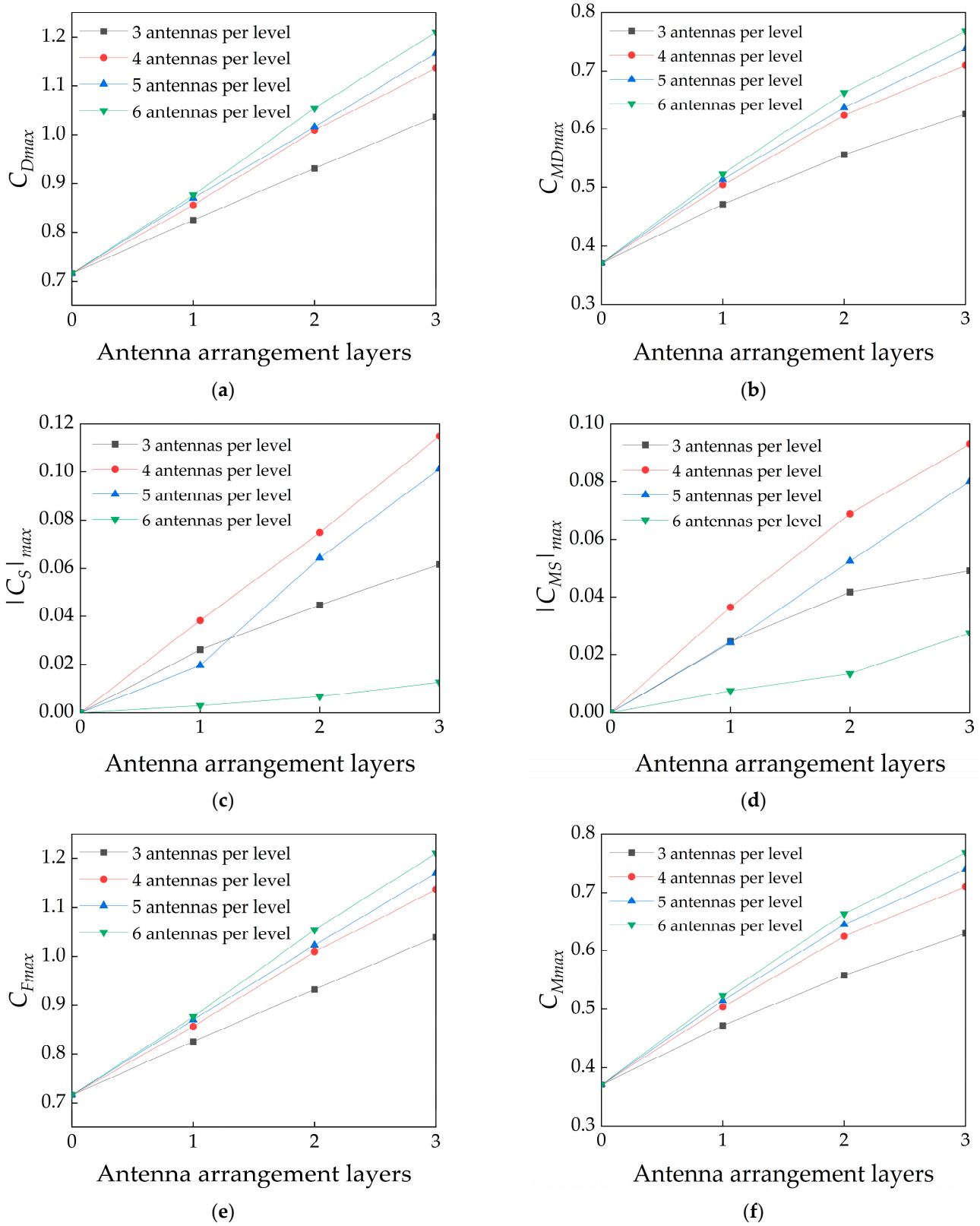

Figure 26. Influence of the antenna arrangement layers on the wind load of the telecommunication tower. (**a**) Drag coefficient. (**b**) Windward base overturning moment coefficient. (**c**) Lateral force coefficient. (**d**) Crosswind base overturning moment coefficient. (**e**) Overturning force coefficient. (**f**) Overturning moment coefficient.

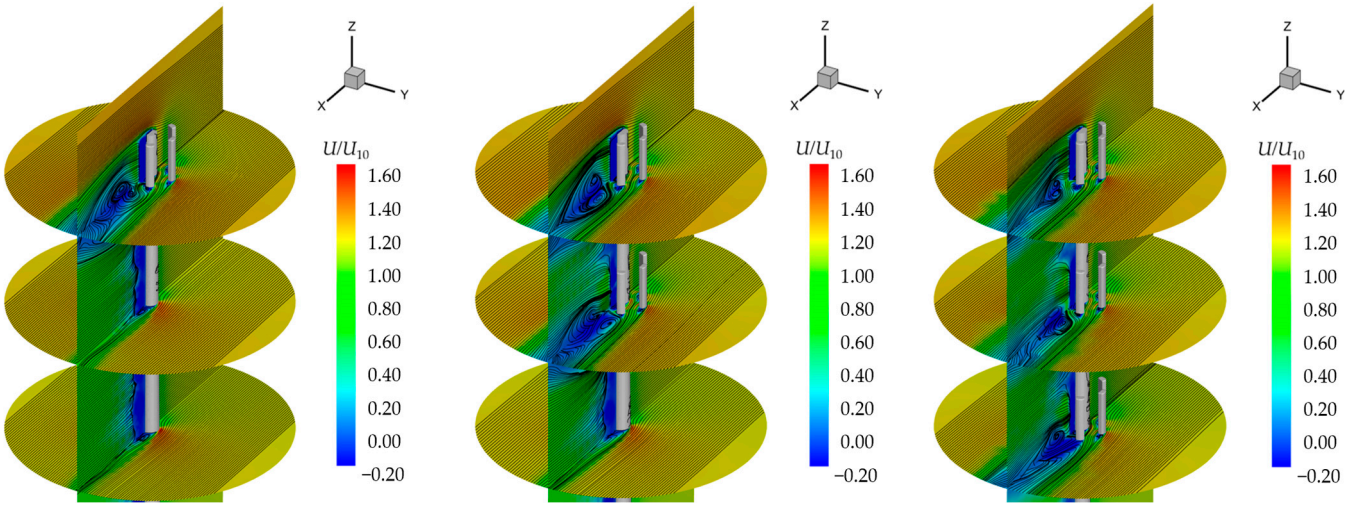

Figure 27. The flow field around the telecommunication tower with 6 antennas per layer, at a wind direction of 30°. (**a**) One layer of antennas. (**b**) Two layers of antennas. (**c**) Three layers of antennas.

Table 4. Maximum values of overturning force coefficient and overturning moment coefficient of the telecommunication tower under all wind directions.

Total Antenna Arrangement Number	Arrangement Parameters			Maximum Values for All Wind Directions		Maximum Values under All Conditions	
	Antenna Arrangement Layers	Arrangement Form	Antenna Arrangement Number per Layer	C_F	C_M	C_{Fmax}	C_{Mmax}
1	1		1	0.77	0.42	0.77	0.42
2	1 1 1	Form 1 Form 2 Form 3	2 2 2	0.81 0.82 0.81	0.45 0.47 0.45	0.82	0.47
3	1		3	0.83	0.47	0.83	0.47
4	1 1 1	Form 1 Form 2 Form 3	4 4 4	0.86 0.85 0.85	0.50 0.50 0.50	0.86	0.50
5	1		5	0.87	0.51	0.87	0.51
6	1 2		6 3	0.88 0.93	0.52 0.56	0.93	0.56
8	2 2 2	Form 1 Form 2 Form 3	4 4 4	1.01 0.98 0.98	0.62 0.60 0.61	1.01	0.62
9	3		3	1.04	0.63	1.04	0.63
10	2		5	1.02	0.64	1.02	0.64
12	3 3 3 2	Form 1 Form 2 Form 3	4 4 4 6	1.14 1.11 1.13 1.05	0.71 0.69 0.71 0.66	1.14	0.71
15	3		5	1.17	0.74	1.17	0.74
18	3		6	1.21	0.77	1.21	0.77

To facilitate practical engineering applications, the least squares method was used to perform a cubic polynomial fit on the maximum overturning force coefficient C_{Fmax} and

the maximum overturning moment coefficient C_{Mmax} from Table 4, yielding corresponding parameter values. These include the first, second, third, and fourth parameter values. This approach provides a reliable basis for the structural design and safety assessment of telecommunication towers in practical engineering.

The wind load fitting formula for the telecommunication tower obtained through numerical fitting is as follows:

$$C_{Fmax} = -5.76 \times 10^{-5} n^3 + 8.70 \times 10^{-4} n^2 + 2.95 \times 10^{-2} n + 0.734 \quad (15)$$

$$C_{Mmax} = -2.01 \times 10^{-5} n^3 - 1.82 \times 10^{-4} n^2 + 3.12 \times 10^{-2} n + 0.383 \quad (16)$$

where n is the total antenna arrangement number.

The data fitting results, as shown in Figures 28 and 29, indicate that the fitting curves for the maximum values of the overturning force coefficient and the overturning moment coefficient have correlation coefficients close to 1.0, demonstrating high conformity with the original data.

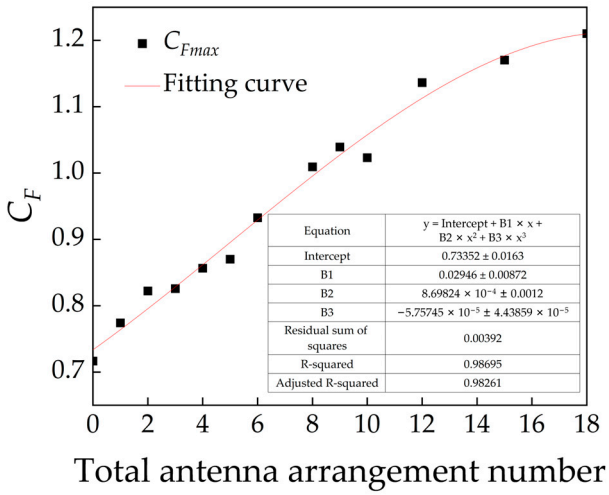

Figure 28. Curve of the maximum overturning force coefficient variation with the total antenna arrangement number.

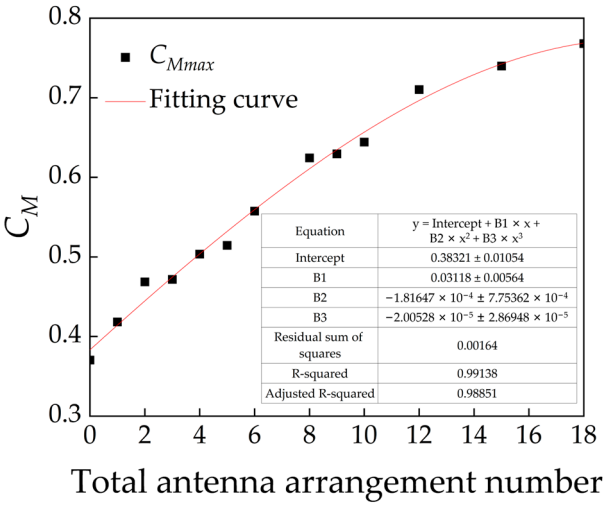

Figure 29. Curve of the maximum overturning moment coefficient variation with the total antenna arrangement number.

4. Conclusions

This study employed three-dimensional numerical simulation methods to systematically investigate the impact of various antenna arrangement parameters, such as the arrangement number, arrangement form, and arrangement layers, on the wind load characteristics of telecommunication towers. It was found that the uniformity of antenna arrangements significantly reduces the sensitivity of the telecommunication tower's wind load to wind direction changes. The lateral force coefficient and the crosswind base overturning moment coefficient are sensitive to changes in the wind direction. With an increase in the antenna arrangement number, the growth rate of the tower's overturning moment coefficient is about twice that of the overturning force coefficient. Additionally, an increase in antenna arrangement layers leads to a linear increase in the tower's overturning force coefficient, whereas the tower's overturning moment coefficient exhibits a nonlinear increase. The rate of increase in the wind load with the antenna arrangement layers is significantly greater than that with the antenna arrangement number. Thus, to reduce wind load, it is advisable in practical engineering applications to increase the antenna arrangement number per layer, thereby reducing the antenna arrangement layers. The study also summarized a calculation method for the structural wind load of telecommunication towers, taking into account the influence of antenna arrangement parameters, providing a reliable basis for the structural design and safety assessment of telecommunication towers in practical engineering.

Author Contributions: Conceptualization, Y.J.; formal analysis, Y.J.; investigation, Z.Z. and M.D.; data curation, J.H., Z.Z. and M.D.; writing—original draft preparation, Y.J. and J.H.; writing—review and editing, Q.L. All authors have read and agreed to the published version of the manuscript.

Funding: This research was funded by the National Natural Science Foundation of China, grant number 52208495, and the Natural Science Foundation of Hebei Province, China, grant number E2021210110.

Institutional Review Board Statement: Not applicable.

Informed Consent Statement: Not applicable.

Data Availability Statement: The raw data supporting the conclusions of this article will be made available by the authors on request.

Conflicts of Interest: The authors declare no conflicts of interest.

References

1. Kim, Y.C. Aeroelastic characteristics of wind turbine with various cross-sectional shape of tower. In Proceedings of the 2021 International Conference on Structural Engineering and Mechanics, Seoul, Republic of Korea, 23–26 August 2021; pp. 24–26.
2. Mannini, C.; Massai, T.; Giachetti, A.; Giusti, A. Aerodynamic loads on groups of offshore wind turbine towers stored on quaysides during the pre-assembly phase. *arXiv* **2023**, arXiv:2302.11018. [CrossRef]
3. Azzi, Z.; Elawady, A.; Irwin, P.; Chowdhury, A.G.; Shdid, C.A. Aeroelastic modeling to investigate the wind-induced response of a multi-span transmission lines system. *Wind. Struct.* **2022**, *34*, 231–257.
4. Prud'homme, S.; Legeron, F.; Langlois, S. Calculation of wind forces on lattice structures made of round bars by a local approach. *Eng. Struct.* **2018**, *156*, 548–555. [CrossRef]
5. Martín, P.; Elena, V.B.; Loredo-Souza, A.M.; Camaño, E.B. Experimental study of the effects of dish antennas on the wind loading of telecommunication towers. *J. Wind. Eng. Ind. Aerodyn.* **2016**, *149*, 40–47. [CrossRef]
6. Torrielli, A.; Giusti, A. Uncertainties in the response of tower-like structures to wind gust buffeting. *J. Wind. Eng. Ind. Aerodyn.* **2023**, *236*, 105404. [CrossRef]
7. Xia, D.; Peng, K. Wind Load and Wind Vibration Response of a TV Tower Based on Force Measurement Test in a Wind Tunnel. *Adv. Civ. Eng.* **2022**, *2022*, 7629438. [CrossRef]
8. Battista, R.C.; Virel Rivero, R.J.; Pfeil, M.S. Aerodynamic Behavior and Stability of the Tall and Slender Brasilia Telecom Tower. *Struct. Eng. Int.* **2022**, *32*, 33–42. [CrossRef]
9. Winterstein, A.; Warnakulasuriya, S.; Bletzinger, K.-U.; Wüchner, R. Computational wind–structure interaction simulations of high rise and slender structures and validation against on-site measurements—Methodology development and assessment. *J. Wind. Eng. Ind. Aerodyn.* **2023**, *232*, 105278. [CrossRef]

10. Cheng, Y.; Dai, K.; Liu, Y.; Yang, H.; Sun, M.; Huang, Z.; Camara, A.; Yin, Y. A method for along-wind vibration control of chimneys by tuning liners. *Eng. Struct.* **2022**, *252*, 113561. [CrossRef]
11. Poddaeva, O.; Fedosova, A. Computational and experimental simulation of wind impacts on a lattice structure. *Energy Rep.* **2023**, *9*, 355–361. [CrossRef]
12. Fu, J.-Y.; Wu, B.-G.; Wu, J.-R.; Deng, T.; Pi, Y.-L.; Xie, Z.-N. Wind resistant size optimization of geometrically nonlinear lattice structures using a modified optimality criterion method. *Eng. Struct.* **2018**, *173*, 573–588. [CrossRef]
13. Ribeiro, D.; Bragança, C.; Montenegro, P.; Carvalho, H.; Costa, B.; Marques, F. Wind-induced fatigue analysis of high-rise guyed lattice steel towers. *Structures* **2022**, *36*, 719–734. [CrossRef]
14. Qin, P.; Zhou, Z. Aerodynamic analysis of the top structure of a monopole telecommunication tower: Impact of wind directions and diameters of the hexadecagonal tube body. *J. Wind. Eng. Ind. Aerodyn.* **2022**, *224*, 104946. [CrossRef]
15. Kumar, M.P.; Raju, P.M.; Navya, M.; Naidu, G. Effect of wind speed on structural behaviour of Monopole and self-support telecommunication towers. *Asian J. Civ. Eng.* **2017**, *18*, 911–927.
16. Belloli, M.; Rosa, L.; Zasso, A. Wind loads on a high slender tower: Numerical and experimental comparison. *Eng. Struct.* **2014**, *68*, 24–32. [CrossRef]
17. Solari, G. Wind loading of structures: Framework, phenomena, tools and codification. *Structures* **2017**, *12*, 265–285. [CrossRef]
18. Wijesooriya, K.; Mohotti, D.; Amin, A.; Chauhan, K. Wind loads on a super-tall slender structure: A validation of an uncoupled fluid-structure interaction (FSI) analysis. *J. Build. Eng.* **2021**, *35*, 102028. [CrossRef]
19. Szafran, J.; Kamiński, M. From full-scale testing of steel lattice towers to stochastic reliability analysis. *Arch. Mech.* **2017**, *69*, 371–388.
20. Zhou, X.; Huang, P.; Gu, M.; Zhu, L.; Pan, H. Wind loads and wind-induced responses of Guangzhou New TV Tower. *Adv. Struct. Eng.* **2010**, *13*, 707–726. [CrossRef]
21. Tanuku, S.; Rama Mohana Rao, K. Assessment of Wind Loads on Lattice Towers Using Various National Standards. In Proceedings of the Emerging Trends in Civil Engineering: Select Proceedings of ICETCE 2018; Springer: Singapore, 2020; pp. 197–208.
22. Hernandez-Estrada, E.; Lastres-Danguillecourt, O.; Robles-Ocampo, J.B.; Lopez-Lopez, A.; Sevilla-Camacho, P.Y.; Perez-Sariñana, B.Y.; Dorrego-Portela, J.R. Considerations for the structural analysis and design of wind turbine towers: A review. *Renew. Sustain. Energy Rev.* **2021**, *137*, 110447. [CrossRef]
23. Malliotakis, G.; Alevras, P.; Baniotopoulos, C. Recent advances in vibration control methods for wind turbine towers. *Energies* **2021**, *14*, 7536. [CrossRef]
24. Raj, T.; Mishra, R.; Kumar, P.; Kapoor, A. Advances in MIMO antenna design for 5G: A comprehensive review. *Sensors* **2023**, *23*, 6329. [CrossRef] [PubMed]
25. Luntovskyy, A.; Spillner, J.; Luntovskyy, A.; Spillner, J. Future mobile communication: From 4G To 5G, 5G enabling techniques. In *Architectural Transformations in NETWORK Services and Distributed Systems*; Springer: Wiesbaden, Germany, 2017; pp. 211–245.
26. Lee, C.-K.; Yu, L. A multi-level perspective on 5G transition: The China case. *Technol. Forecast. Soc. Chang.* **2022**, *182*, 121812. [CrossRef]
27. Horst, H.A.; Foster, R.J. 5G and the digital imagination: Pacific Islands perspectives from Fiji and Papua New Guinea. *Media Int. Aust.* **2023**, *190*, 54–67. [CrossRef]
28. Wang, J.; Jiao, Z.; Wang, Q.; Zhu, Y.; Li, K. Analysis of novel 5G wireless communication coverage enhancing service mode with power towers and street lamp poles integrated. In Proceedings of the 2022 IEEE 6th Information Technology and Mechatronics Engineering Conference (ITOEC), Chongqing, China, 4–6 March 2022; pp. 1215–1220.
29. Lun, J.; Frenger, P.; Furuskar, A.; Trojer, E. 5G new radio for rural broadband: How to achieve long-range coverage on the 3.5 GHz band. In Proceedings of the 2019 IEEE 90th Vehicular Technology Conference (VTC2019-Fall), Honolulu, HI, USA, 22–25 September 2019; pp. 1–6.
30. Dangi, R.; Lalwani, P.; Choudhary, G.; You, I.; Pau, G. Study and investigation on 5G technology: A systematic review. *Sensors* **2021**, *22*, 26. [CrossRef] [PubMed]
31. *GB 50009-2012*; Load Code for the Design of Building Structures. Ministry of Housing and Urban-Rural Development of the People's Republic of China: Beijing, China, 2012.
32. Zeng, Y.; Wang, H.; Sun, M.; Wang, C.; Liu, X. SST turbulence model improvements: Review. *Acta Aeronaut. Astronaut. Sin.* **2023**, *44*, 27411. [CrossRef]
33. Menter, F.R. Two-equation eddy-viscosity turbulence models for engineering applications. *AIAA J.* **1994**, *32*, 1598–1605. [CrossRef]
34. Wang, H.; Zhang, B.; Qiu, Q.; Xu, X. Flow control on the NREL S809 wind turbine airfoil using vortex generators. *Energy* **2017**, *118*, 1210–1221. [CrossRef]